



Programme: ELT

Project: ELT MCAO Construction – MORFEO




MORFEO Calibration Unit Optomechanical System – OFDR Design and Analysis Report

Document Number: E-MAO-PU0-INA-DER-002

Document Version: 01

Document Type: Design Report (DER), Analysis Report (ANR)

Released On: 2024-11-22

	Name	Signature	Date
Owner:	Gianluca Di Rico		2024-11-22
Approved by PI:	Paolo Ciliegi		2024-11-22
Released by PM:	Andrea Di Rocco		2024-11-22





Authors

Name	Affiliation
Ivan Di Antonio	INAF – OAAb
Gianluca Di Rico	INAF – OAAb
Gabriele Rodeghiero	INAF – OAS / OAAb
Mauro Dolci	INAF – OAAb
Benedetta Di Francesco	INAF – OAAb
Angelo Valentini	INAF – OAAb



Table of contents

Table of contents	3
1. Introduction.....	5
1.1 Content	5
1.2 Common definitions, acronyms and abbreviations.....	5
2. Related documents	8
2.1 Applicable Documents	8
2.2 Reference Documents	8
3. Overview	9
4. Optical design review	10
4.1 Preliminary optical design review	10
4.1.1 Cube Beam Splitter	11
4.1.2 Opto-mechanical aspects.....	12
4.1.3 LGS arm	13
5. New optical layout (OFDR)	15
5.1 Nominal performances	18
5.1.1 NGS sources	18
5.1.2 LGS sources.....	21
5.1.3 Summary	24
5.2 WFE budget.....	25
5.2.1 Sensitivity analysis	25
5.2.2 Tolerance analysis (MonteCarlo)	27
5.2.3 Thermal aspects.....	32
5.2.4 WFE breakdown.....	32
5.2.5 WFE compensation strategy	33
5.3 Pupil quality	39
5.3.1 Tolerance analysis	40
5.4 F-number	44
5.5 Ghosts and stray light.....	44
5.5.1 Ghost PDR analysis summary	45
5.5.2 Stray light PDR analysis summary.....	45
5.5.3 Additional ghost analyses for OFDR	46
5.6 Optical alignment.....	49
6. Mechanical design review	50
6.1 Preliminary mechanical design review	50
6.2 The new mechanical concept.....	50
6.2.1 Structure	50
6.2.2 NGS mask assembly (NGSM)	52



6.2.3 LGS mask assembly (LGSM).....	56
6.2.4 Pupil Sources Assembly (PSA).....	58
6.3 Structural aspects.....	58
6.4 Opto-mechanical aspects.....	60
7. Throughput analysis.....	64
7.1 NGS path.....	64
7.2 LGS path.....	65
7.3 Throughput summary.....	66
7.4 Lamps power and flux compliance.....	66
8. Test Equipment.....	69
9. Technical Risk Analysis.....	71
9.1 Ghost analysis.....	71
9.2 Stray-Light analysis.....	72
9.3 Throughput analysis.....	72
9.4 CBS quality and procurement.....	73
9.5 Thermal effects.....	73
9.6 Coatings.....	73
9.7 Window aspect ratio.....	74
9.8 Alignment of W-SM.....	74
10.Verification Matrix.....	76
11.Conclusion.....	77



1. Introduction

1.1 Content

This document resumes the design solutions adopted for the MORFEO Calibration Unit Optomechanical System (PUA), reports the main analyses performed to verify the compliance with the main specifications and describes the main risks and related mitigation strategies, in the framework of the subsystem Optical FDR (OFDR).

1.2 Common definitions, acronyms and abbreviations

AD	Applicable Document
AIV	Assembly, Integration and Verification
AO	Adaptive Optics
ARR	Acceptance Readiness Review
A.U.	Arbitrary Unit
BIH	Bologna Integration Hall
BW	Bandwidth
CoG	Center of Gravity
CTE	Coefficient of Thermal Expansion
CU	Calibration Unit
CUFM	Calibration Unit Folding Mirror
ELT	European Extremely Large Telescope
ESO	European Southern Observatory
DL	Diffraction Limited
DM	Deformable Mirror
FDR	Final Design Review
FoV	Field of View
FWHM	Full Width at Half Maximum
HW	Hardware
ICD	Interface Control Document
ICH	Instrument Control Hardware
ICS	Instrument Control System
INAF	Istituto Nazionale di AstroFisica
INS	Instrumentation Software
INSU	Institut National des Sciences de l'Univers
IORR	Instrument Operations Readiness Review
IPAG	Institut de Planétologie et d'Astrophysique de Grenoble
IRD	Interface Requirement Document
LFP	Laser Focal Plane
LGS	Laser Guide Star



LOR	Low Order and Reference
LUT	Look-Up Table
MAIT	Manufacturing Assembly Integration and Test
MAT	Micro-Alignment Telescope
MORFEO	Multiconjugate adaptive Optics Relay For ELT Observations
MCAO	Multi Conjugate Adaptive Optics
MICADO	Multi-AO Imaging Camera for Deep Observations
MFD	Mode Field Diameter
MMF	Multi-Mode Fiber
MOA	MORFEO Optical Alignment
MS	Main Structure
N/A	Not Applicable
NA	Numerical Aperture
NCPA	Non-Common Path Aberrations
NDF	Neutral Density Filter
NGS	Natural Guide Star
NUIG	School of Physics at the National University of Ireland Galway
OAAb	Osservatorio Astronomico d'Abruzzo
OAS	Osservatorio di Astrofisica e Scienza dello Spazio di Bologna
OD	Optical Density
OFDR	Optical Final Design Review
PAC	Percentage Area Coverage
PAC	Preliminary Acceptance Review in Chile
PAE	Preliminary Acceptance Europe
PPS	Pupil Point Source
PCUP	Paraxial Calibration Unit Prototype
PDR	Preliminary Design Review
PFRO	Post-focal Relay Optics
PI	Principal Investigator
PM	Pupil Mirror
PSF	Point Spread Function
PT	Product Tree
PU0	MORFEO Calibration Unit subsystem/work-package
PUA	MORFEO Calibration Unit Optomechanical System
PUB	MORFEO Calibration Unit Electronic Cabinet
PV	Peak-to-Valley
QE	Quantum Efficiency
RAMS	Reliability, Availability, Maintainability and Safety
RD	Reference Document
RMS	Root Mean Square
RoC	Radius of Curvature
RON	Read Out Noise
RSS	Root Sum Squared



RTC	Real-Time Computer
SA	Sub-Aperture
SAG	Sagitta
SAT	System Architect Team
SCAO	Single-Conjugate Adaptive Optics
SE	System Engineer
SET	System Engineering Team
SL	Stray Light
SMF	Single-Mode Fiber
SNR	Signal to Noise Ratio
SOW	Statement of Work
SR	Strehl Ratio
SRR	System Requirements Review
SW	Software
TAC	Test & Alignment Camera
TBC	To Be Confirmed
TBD	To Be Defined
TBE	To Be Evaluated
TBW	To Be Written
TIS	Total Integrated Scatter
TFP	Telescope Focal Plane
WFE	Wavefront Error
WFS	Wavefront Sensor
WL	Wavelength
WP	Work Package



2. Related documents

2.1 Applicable Documents

The following applicable documents form a part of the present document to the extent specified herein. In the event of conflict between applicable documents and the content of the present document, the content of the present document shall be taken as superseding.

- AD1 E-MAO-PU0-INA-ICD-002_01 MORFEO Calibration Unit Optomechanical System – Optical Interfaces
- AD2 E-MAO-PU0-INA-PLA-002_01 MORFEO Calibration Unit Optomechanical System – OFDR Alignment Plan
- AD3 E-MAO-PUA-INA-MOD-001_01 MORFEO Calibration Unit – Optical Model (direct)

2.2 Reference Documents

The following documents, of the exact version shown herein, are listed as background references only. They are not to be construed as a binding complement to the present document.

- RD1 E-MAO-PU0-INA-ANR-002_01 MORFEO Calibration Unit – OFDR WFE budget
- RD2 E-MAO-PUA-INA-MOD-002_01 MORFEO Calibration Unit Optomechanical System – Preliminary Mechanical Model
- RD3 E-MAO-PU0-INA-TNO-002_01 MORFEO Calibration Unit Optomechanical System – Preliminary Optical Prescriptions



3. Overview

The MORFEO Calibration Unit subsystem (PU0) will be installed at the entrance port of MORFEO and will project different types of calibration sources to provide reference light to multiple sensors and instruments, such as the NGS and LGS wavefront sensors (WFSs), and also focal plane instruments attached to the exit port of MORFEO, such as MICADO. The calibration sources, both diffraction-limited and extended sources, providing light from visible to near infrared wavelengths, will help to calibrate the non-common path aberrations (NCPA), to perform system and subsystem functional and health checks, and to train the tomographic reconstructor.

The Calibration Unit (CU) can be used in daytime and night-time, before starting the observations. Moreover, before installation on the telescope Nasmyth platform, it will enable calibration of MORFEO during the AIV phase while being integrated in Europe, as a Test Unit by simply exchanging the fixed Pupil Mirror (PM) with a deformable one (DM).

Three main light sources will be provided by the CU and projected into MORFEO:

- Diffraction-limited, near-infrared (H-band) sources, conjugated at infinity, to feed the low-order WFSs located within the ELT technical field of view (FoV) and the MICADO science FoV.
- Extended, seeing-limited, NGS reference sources (R-band), to feed the high-order, reference WFSs located within the ELT technical FoV.
- Extended LGS sources (589 nm) to feed the LGS WFSs, at two different conjugated altitudes (104 km and 150 km).

The main purposes of the calibration sources are:

- NGS-REF sources: to map field distortions in the R-band with well sampled PSFs.
- NGS-LO sources: to calibrate low-order aberrations and simulate different anisoplanatic angles.
- NGS-MIC sources: to calibrate NCPA between the MICADO focal plane and the NGS WFSs.
- LGS sources: to calibrate the LGS WFSs.

The Calibration Unit will reproduce the ELT optical interfaces (such as f-number and exit pupil position), to fully simulate the telescope performances and residual aberrations (e.g., in the LGS path).

The Calibration Unit Optomechanical System (PUA), directly integrated into MORFEO, contains most of the optical and mechanical components of the Calibration Unit and is the subject of this report.

The PUA will be fed through optical fibers from the Calibration Unit Electronic Cabinet (PUB), where all the light sources are integrated. All the power systems and control electronics will be installed inside this cabinet, sitting at the Nasmyth platform, and interfaced to the PUA via dedicated cables. The light from the PUA will be directed upward, through the (exit) Window (W), towards a deployable folding mirror (CUFM), and then into MORFEO. The CUFM, while belonging to the Calibration Unit optical path illuminating the MORFEO optics, does not belong to the Calibration Unit work-package (PU0). However, being a flat mirror and placed close to the NGS focal plane, it will mostly affect the LGS beams and the exit pupil position. Its contribution to the overall WFE budget is not directly considered in this report.



4. Optical design review

4.1 Preliminary optical design review

An initial analysis of the preliminary optical design (Figure 1) was aimed at verifying the main features of the PUA, including its performances in terms of wavefront error (WFE), and how it depends on the optical tolerances at component level during their manufacture, integration and alignment.

Some areas were identified as critical:

- (a) The Cube Beam Splitter (CBS) had very tight manufacturing tolerances, unlikely to be met, including the reflected/transmitted WFE, due to unavoidable inhomogeneity within the glass blank, surface irregularities, and the 50:50 beam-splitter coating.
- (b) The clearances between optical and mechanical components were quite small, making their assembly and alignment impractical.
- (c) LGS optics were not optimized for a (small) wavelength range, but only at a single wavelength, making it very sensitive to changes in the central wavelength of the adopted LGS light source and its bandwidth.
- (d) LGS nominal WFE was changing significantly between the two conjugated altitudes, taking a large fraction of the allocated WFE budget.
- (e) The “Telescope” optics, i.e. the Window (W) and the Spherical Mirror (SM), were quite heavy.
- (f) The gravity orientation of many optical components, such as the 45° beam-splitters, was not optimal, thus introducing gravity sag effects, difficult to be reduced or controlled.
- (g) Some lenses have edges that were too thin.

In the following sections the main concerns are described in more detail.

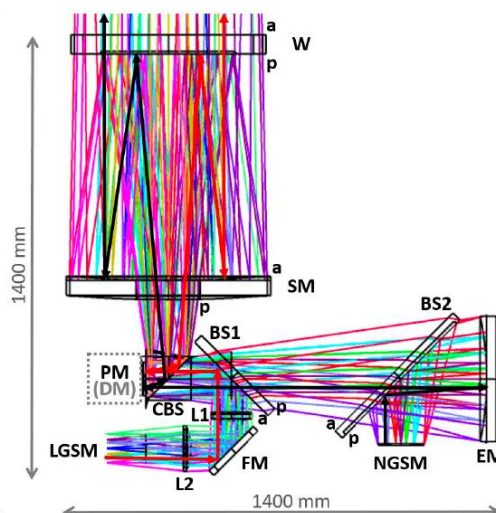


Figure 1. PUA preliminary optical design. Black and red arrows identify the nominal optical paths, NGS and LGS, respectively.



4.1.1 Cube Beam Splitter

The Cube Beam Splitter (CBS) is quite bulky and the average optical path inside the CBS is roughly 300 mm. Even assuming the best available glass material, with a homogeneity $\Delta n=1$ part per million (ppm), it will translate into a WFE ($\Delta n \cdot d$) of ~ 300 nm (PV), with an expected value of 30-40 nm rms, after focus subtraction. Moreover, temperature changes (spatial gradients) will add their own contribution to the WFE budget in an unpredictable way, unless thermal gradients are carefully controlled and minimized. Currently, the CBS material (N-BK7) has quite a low sensitivity to thermal gradients via the change of the refractive index with temperature (dn/dT), lower than many other optical materials. Fused Silica is considered as a valid alternative, with a higher homogeneity grade normally achievable. Preliminary inquiries with potential vendors for raw materials have shown that no supplier will guarantee the homogeneity level of 1 ppm in all directions (not even for Fused Silica), but only in one direction, with the other two at lower grades. It may therefore be expected that the overall WFE will be even higher than the previous estimate.

Here are some mitigating strategies:

- Because the entrance 45° prism will be crossed only once, and in one direction only, it is advisable to cut and integrate the prism along the best direction.
- The second prism will be crossed three times, twice in double-pass, in the horizontal direction, and a third one, after being reflected, in the vertical. Again, it is better to select the best axis as the horizontal one.
- Because both prisms will have the same size and shape, it is quite possible to inspect some different blanks before allocating which of them will be used for the first or the second prism. Having some spare blanks will also help.
- The 50:50 beam-splitter coating design will be required to minimize reflected and transmitted WFEs as part of its optimization.
- To minimize the effect of thermal gradients, BK7 is the preferred choice, even if its homogeneity grade can be worse than Fused Silica. However, homogeneity is a fixed (stationary) WFE pattern that can be measured and compensated by applying a correction map on the Pupil Mirror (PM) – or the deformable mirror (DM) in TU configuration. This map, being applied to a pupil plane, will correct only common-mode aberrations (those ones that are invariant with field position), likely low-order modes only. This compensation strategy, described in Section 5.2.5, actually applies to the fully integrated system, thus compensating for more than just the effects of the single component.
- Thermal straps and proper thermal modelling can help to reduce gradients inside the prism, or to reduce the cooling/warming time. Temperature probes around the CBS could help to find when thermal gradients are small enough to execute better calibration observations.

Figure 2 shows the sectional view of the ray-tracing close to the CBS, where it is quite evident that the entrance side (on the right) and the exit side (on the top) are left with basically no margin between the mechanical aperture and the clear (effective) aperture, and also for the required protective chamfers/bevels. Its current size ($140 \times 140 \times 140 \text{ mm}^3$) needs to be increased to $150 \times 150 \times 150 \text{ mm}^3$.

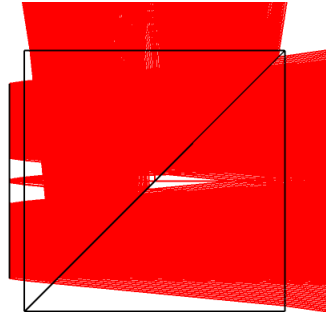


Figure 2. Ray-tracing for a (140x140x140) mm³ CBS.

4.1.2 Opto-mechanical aspects

Figure 1 shows the crowded layout of the PUA preliminary optical design. The clearance between many optical elements and their mounts is very limited. Below the SM, many large optical components and subsystems have been packed closely together. This makes the opto-mechanical design quite challenging. Moreover, there are very small margins between optical beams, mechanical components, and, for each optical component, between their mechanical apertures and their clear effective apertures. Due to the tight overall volume constraints, it can be difficult to accommodate for any change in this configuration. Moreover, the limited clearance will involve difficulties during the integration and alignment phases, increasing the possibility of collisions during those processes, this increasing the risks of damaging expensive and delicate optical components. It also makes any cleaning impractical without dismounting. Another further aspect is the possibility of unwanted stray light sources, because there is no space to add baffles and vanes to prevent and limit the visibility of mechanical surfaces (critical surfaces) or to avoid shining unwanted light on them (illuminated surfaces). These are the main reasons to look for an alternative layout, by changing orientation of the optical components, their clearance, and position in space.

Both the semi-reflective flat Window (W) and the Spherical Mirror (SM) are relatively large and heavy components (W has a diameter of 640 mm and a thickness of 60 mm, SM has a diameter of 670 mm and a thickness of 60 mm), fully suffering from gravity sag effect. While this effect can be minimized through a careful design of their opto-mechanical mountings, this will translate into mildly complex subsystems, requiring proper space and weight allocations. It is thus desirable to try to minimize their weight, by making both of them thinner, with a benefit also for the opto-mechanics. In fact, even if thinner elements will suffer more from gravitational deformations, a proper opto-mechanical design ensures that most of those deformations are axisymmetric (defocus, spherical aberration) so that they can be partially compensated during the system alignment. From the manufacturing point of view, there is a limit to the minimum thickness: this value is smaller for W and larger for SM.

Finally, two large optical components, namely the two plano beam-splitters BS1 and BS2, are oriented at 45° with respect to the gravity vector. They will therefore suffer from asymmetric gravity sag variations, due their elliptical shape, limited thickness and the constraint to have them attached only along their periphery.



4.1.3 LGS arm

The current LGS arm design has been optimized for a single wavelength (589 nm). While this choice matches the monochromatic nature of the final laser beam, other quasi-monochromatic sources could be used, like LEDs or other broadband sources coupled with narrowband filters. In order to maximize the number of useful photons, the band-pass FWHM cannot be too small. In this case, if the LGS optics are not properly achromatic, chromatic aberrations will show up, introducing another wavefront error source and spreading light over a larger spot, thus reducing its intensity. This can be shown by looking at the spot diagrams over a 10 nm band-pass and at the polychromatic WFE maps (Figure 3 and Figure 4).

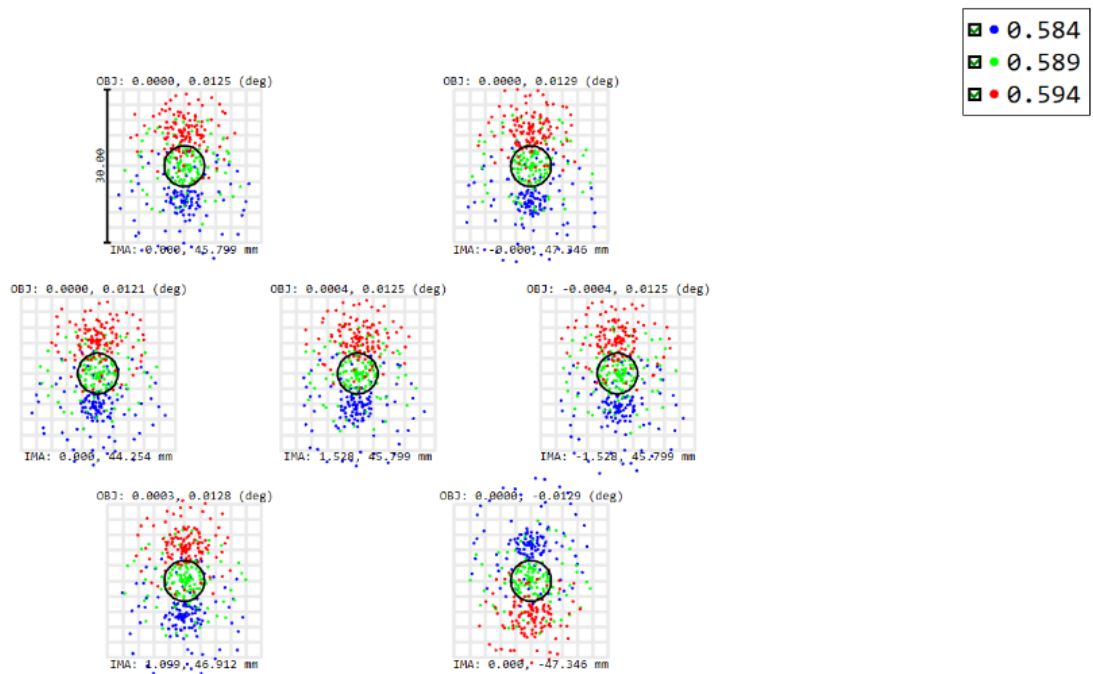


Figure 3. PUA preliminary design optical performance: LGS spot diagrams conjugated at 104 km.

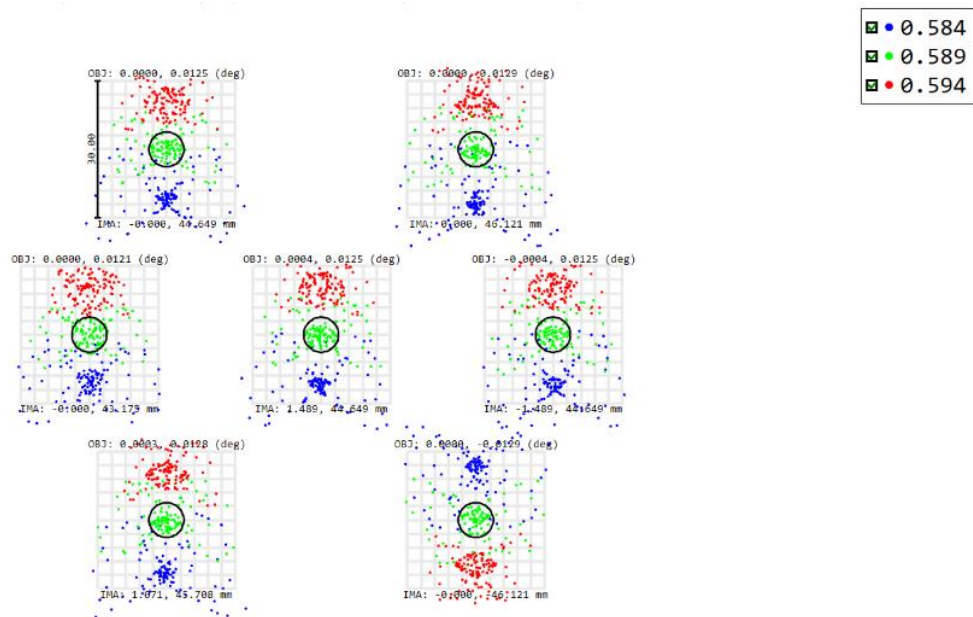


Figure 4. PUA preliminary design optical performance: LGS spot diagrams conjugated at 150 km.

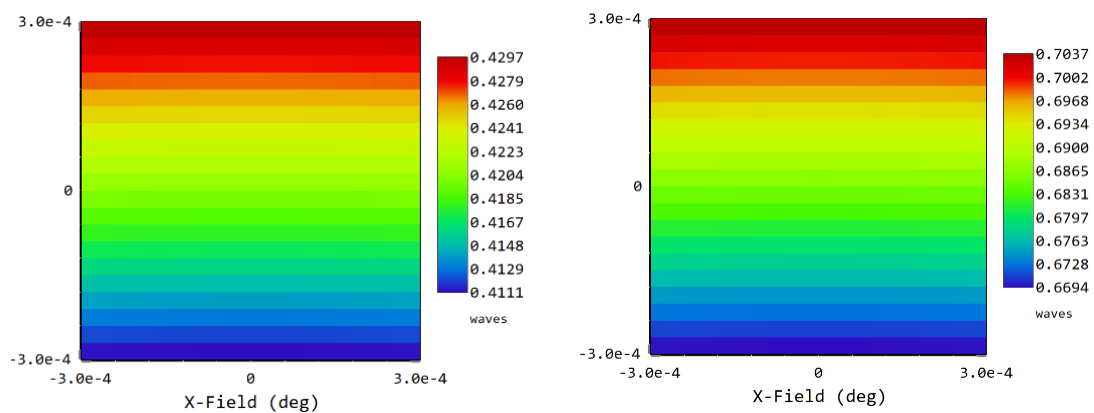


Figure 5. PUA preliminary design optical performance: LGS WFE map over 2''x2'' field of view, conjugated at 104 km (left) and 150 km (right).

From these plots it is quite evident that a lot of blur (mostly lateral color) develops if LGS light sources are not monochromatic. To fix this issue, the LGS optics must be redesigned to make the arm achromatic (changing lenses from singlets to achromatic doublets). It is also evident that there is a quite large variation of the WFE as a function of the conjugated altitude (Figure 5). Some attempts to reduce this effect would help to match the required WFE budget.



5. New optical layout (OFDR)

To overcome most of the concerns reported in the previous section, a new optical layout has been developed (Figure 6, Figure 7, Figure 8, Figure 9).

The main changes are:

- The location of the optical components inside the available volume has been modified to increase their clearances.
- The thickness of W and SM have been reduced to 30 and 50 mm, respectively.
- The CBS is larger: 150 x 150 x 150 mm³.
- BS1 and BS2 have been rotated by 90° along the horizontal axis to make them unaffected by gravity.
- The LGS arm is now folded towards the Ellipsoidal Mirror (EM).
- BS1 and BS2 are now wedged by ~1°, improving NGS channel image quality and reducing double-bounce ghosts produced by the previous parallel plano surfaces placed on a collimated beam.
- BS1 is now a dichroic Beam Splitter.
- LGS lenses have been redesigned to be achromatic within a 584-594 nm band and improve their nominal image quality (smaller WFE) for both conjugated altitudes (104 and 150 km).

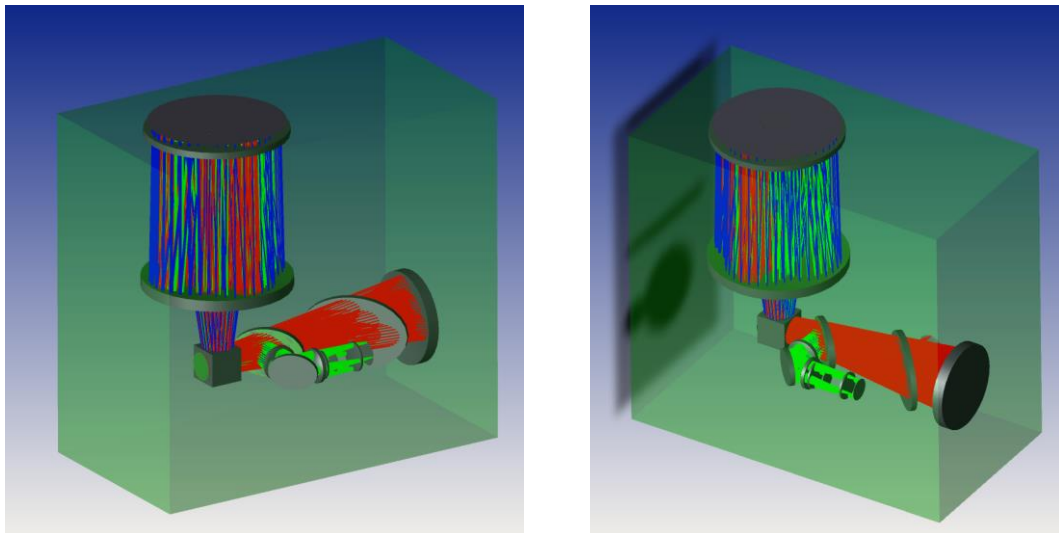


Figure 6. The new PUA optical layout inside the available volume.

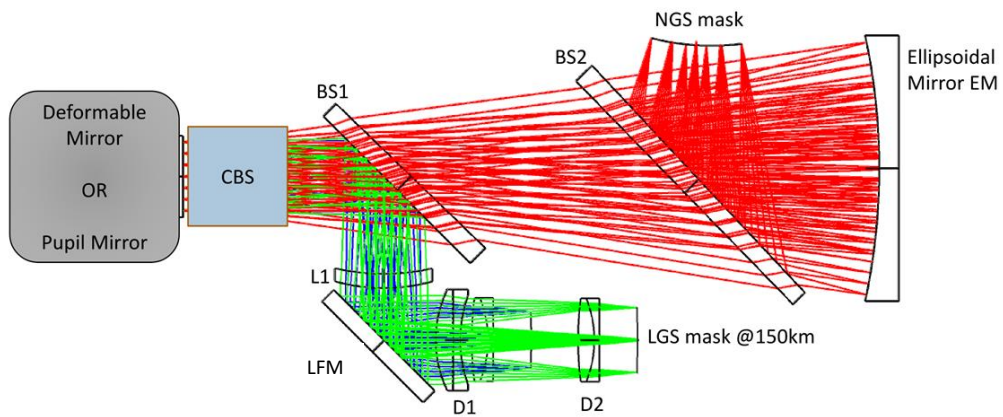


Figure 7. Top view (XY plane) of the new PUA optical layout: components positioned below W and SM.

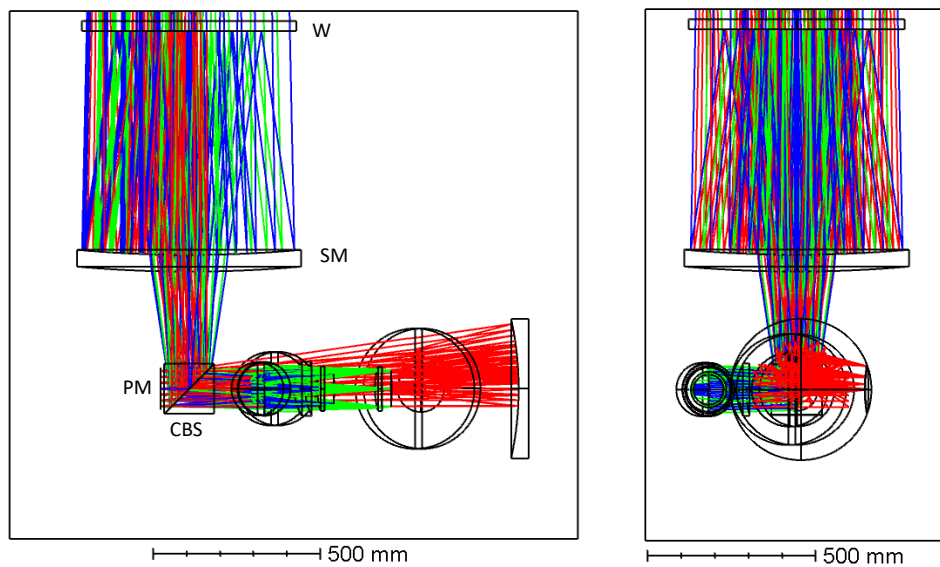


Figure 8. The new PUA optical layout: front view (YZ plane, left) and lateral view (XZ plane, right).

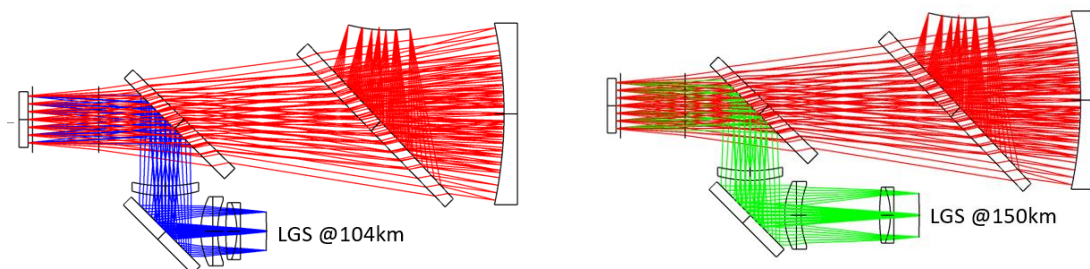


Figure 9. Top view (XY plane) of the new PUA optical layout: the two LGS configurations.



The new LGS arm (Figure 9) is based on one single lens (L1) and two achromatic doublets (D1, D2). Only one aspherical surface has been retained – the surface of D1 close to the LGS folding mirror (LFM) – reducing its maximum aspherical sag departure from the best fit sphere to 52 μm (Figure 10). The second doublet (D2) is stationary with respect to the LGS mask, i.e. moving jointly with the mask. Only standard, easily available glasses have been chosen, to facilitate their manufacturability. The beam is also nearly telecentric at the LGS mask and the design has been optimized for a 3" FoV (centered at 45" off-axis) and to avoid tight manufacturing and alignment tolerances.

The travel range between the two different conjugated altitude configurations has increased to 165 mm, requiring a linear stage with a longer stroke.

The main characteristics of the new design optical components are reported in Table 1, the optical drawings are given in RD3.

Table 1. List of the new design optical components with the main optical and mechanical characteristics. The items marked with an asterisk have one aspherical surface. Units are mm.

Name	Name / Description	Aperture type	Substrate aperture	Central thickness	RoC	Material
W	(semi-reflecting) Window	Circular	Ø640	30	infinity	Fused Silica
SM	(semi-reflecting) Spherical Mirror	Circular	Ø670	50	3700 3700	Fused Silica
PM*	Pupil Mirror	Circular	Ø120	20	infinity	Zerodur
CBS	Cube Beam Splitter	Square	150 x 150	150	infinity	N-BK7 or Fused Silica
BS1	Beam Splitter #1	Elliptical	320 x 220	30	infinity	Fused Silica or N-BK7
BS2	Beam Splitter #2	Elliptical	480 x 330	30	infinity	Fused Silica or N-BK7
EM*	Ellipsoidal Mirror	Circular	Ø420	35	974.75	Zerodur
L1	(Lgs) Lens #1	Circular	Ø154	22	-279.24 -336.91	S-BSL7
D1*	(Lgs) Doublet #1	Circular	Ø156	38	-203.52 infinity -174.63	S-BSL7 S-NSL36
D2	(Lgs) Doublet #2	Circular	Ø132	33	Infinity 172.80 -502.82	S-LAL18 S-TIH14
LFM	(Lgs) Folding mirror	Elliptical	220 x 160	25	infinity	Zerodur

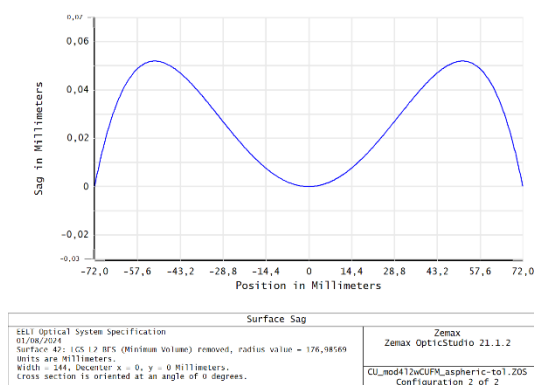


Figure 10. The aspheric surface of D1: sag departure from best-fit-sphere (max 52 μm).

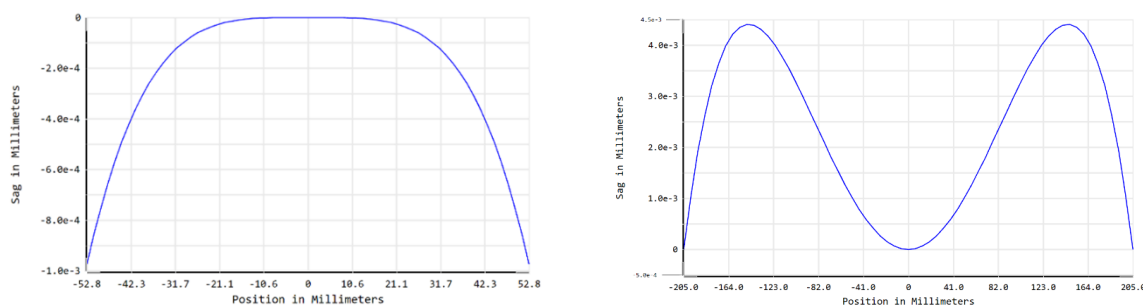


Figure 11. The aspheric surface of PM (left) and EM (right): sag departure from best-fit-sphere (max 1 μm and 4.5 μm , respectively).

5.1 Nominal performances

The new PUA design, proposed as a result of the analysis of the criticalities, was optimized for as-built performance, by examining the optical tolerances and reducing sensitivities to manufacture, integration, and alignment errors. The following sections describe the nominal performance, while the as-built performance resulting from sensitivity and tolerance analyses, carried out mainly looking at the WFE budget, is described in Section 5.2.

5.1.1 NGS sources

The NGS image quality has been analyzed in terms of spot size and WFE, as measured using the reverse ray-tracing model, including the ELT telescope optics down to the NGS / LGS focal planes of the PUA. Spot diagrams are given in Figure 12 and Figure 13 for H-band and R-band, respectively. The black circles represent the size of the Airy disk, showing that the geometrical spot size is much smaller than diffraction. Moreover, lateral color has been minimized. Figure 14 shows a comparison between the spot size of the preliminary and the new PUA designs, plotted with the same plate scale: the net gain is evident.

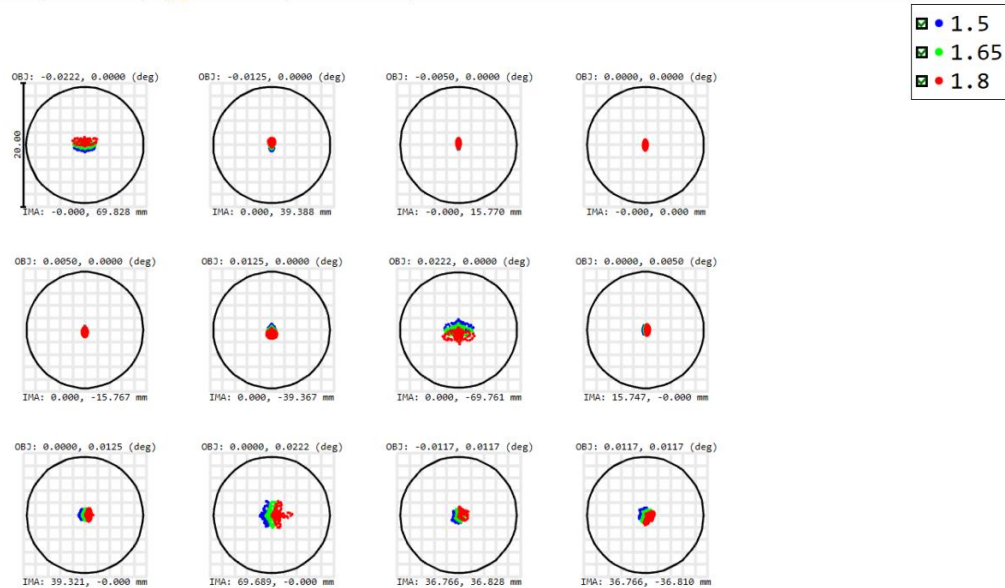


Figure 12. New PUA design: NGS spot diagrams, H-band.

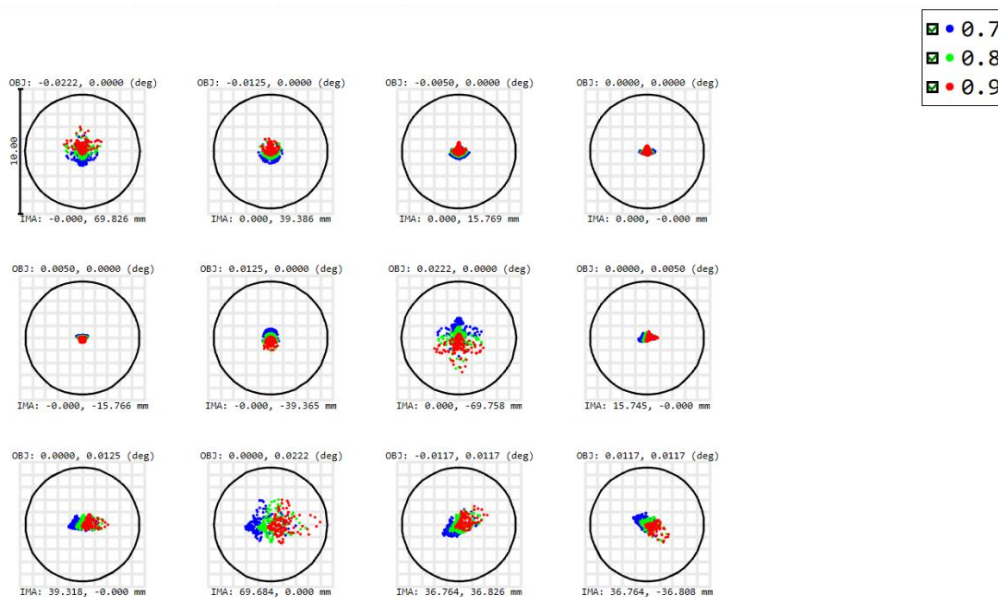
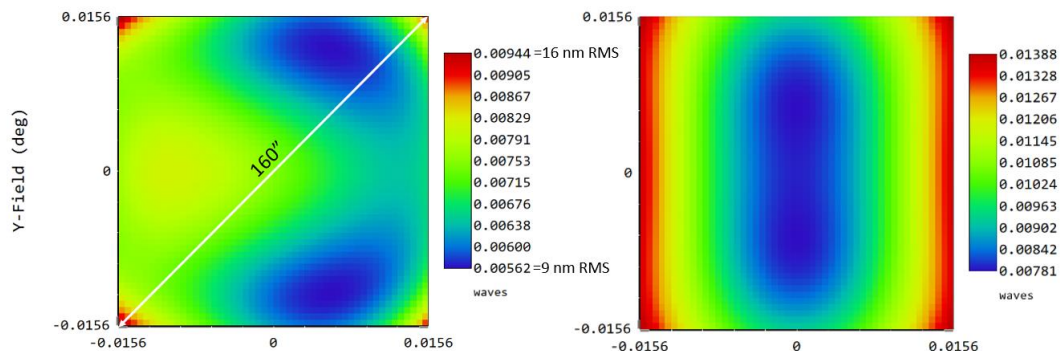


Figure 13. New PUA design: NGS spot diagrams, R-band.



Figure 14. NGS spot diagrams comparison between the two PUA designs: new design (left) and preliminary design (right).

Figure 15 shows a comparison of the WFE (rms) field maps in the H-band for the preliminary PUA design and the new design. Both the technical FoV and the smaller MICADO FoV maps are given. Figure 16 shows a similar comparison in the R-band in the MORFEO technical FoV.



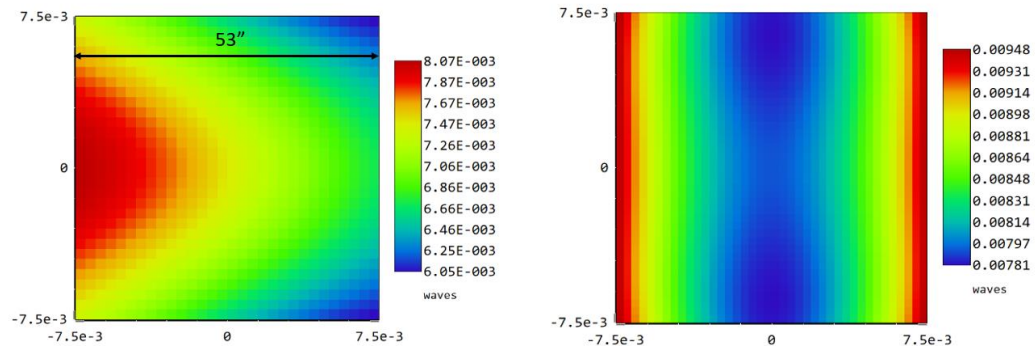


Figure 15. Maps of the WFE (rms) for NGS sources over the technical (top) and MICADO (bottom) FoV in H-band: new design (left) and preliminary design (right).

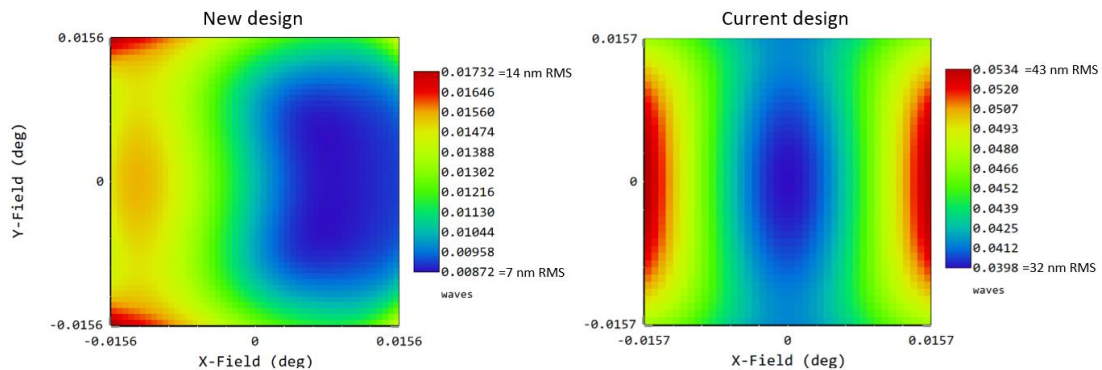


Figure 16. Maps of the WFE (rms) for NGS sources over the technical FoV in R-band: new design (left) and preliminary design (right).

5.1.2 LGS sources

The image quality of the LGS sources is given by spot diagrams and WFE field maps for both conjugated altitudes. Figure 17 and Figure 18 show the spot diagrams for the LGS sources, in the reverse ray-tracing model, starting from the atmosphere, through the ELT telescope, and down to the PUA LGS focal plane.

A comparison of the LGS spot sizes for the two PUA designs is given in Figure 19. The new design improves the image quality of the two LGS configurations by a large factor, removing the lateral color. This is also demonstrated by the field maps of the WFE rms values given in Figure 20 and Figure 21.

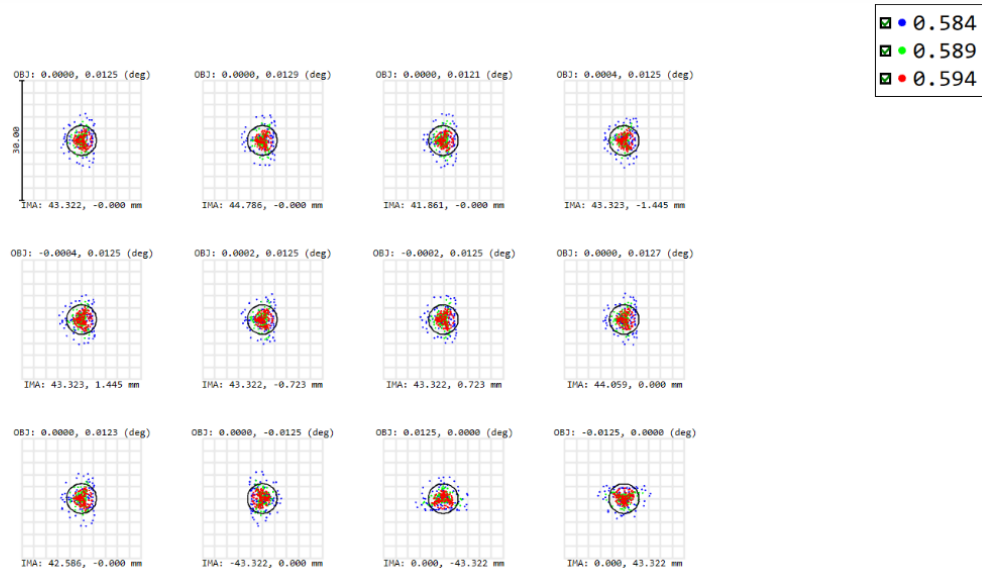


Figure 17. New PUA design LGS spot diagrams for 104 km conjugation altitude.

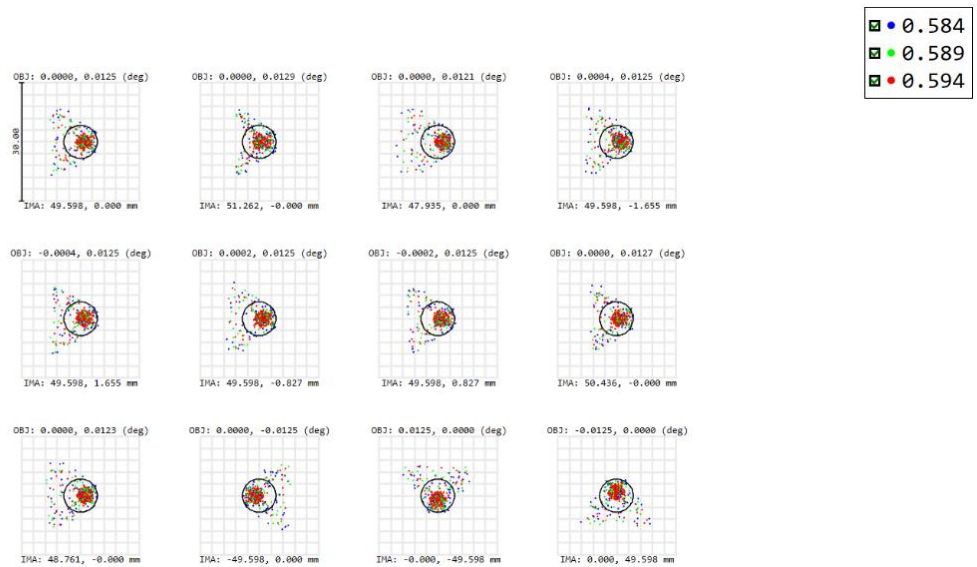


Figure 18. New PUA design LGS spot diagrams for 150 km conjugation altitude.

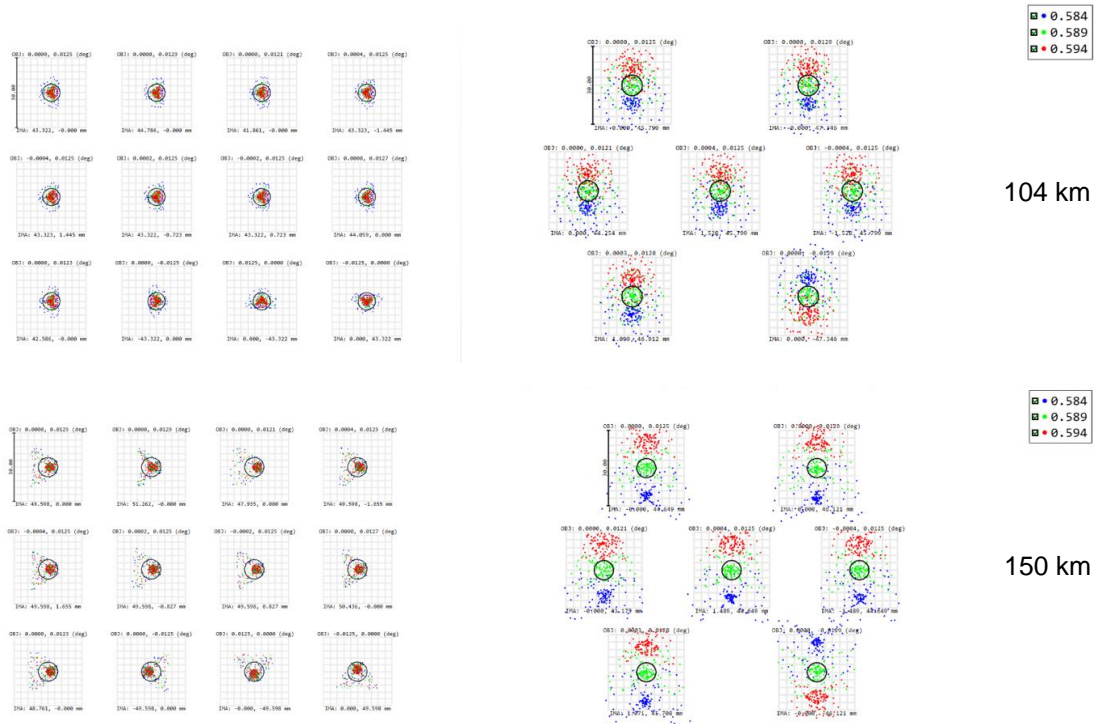


Figure 19. LGS spot diagrams. Comparison between the two PUA designs: new design (left) and preliminary design (right).

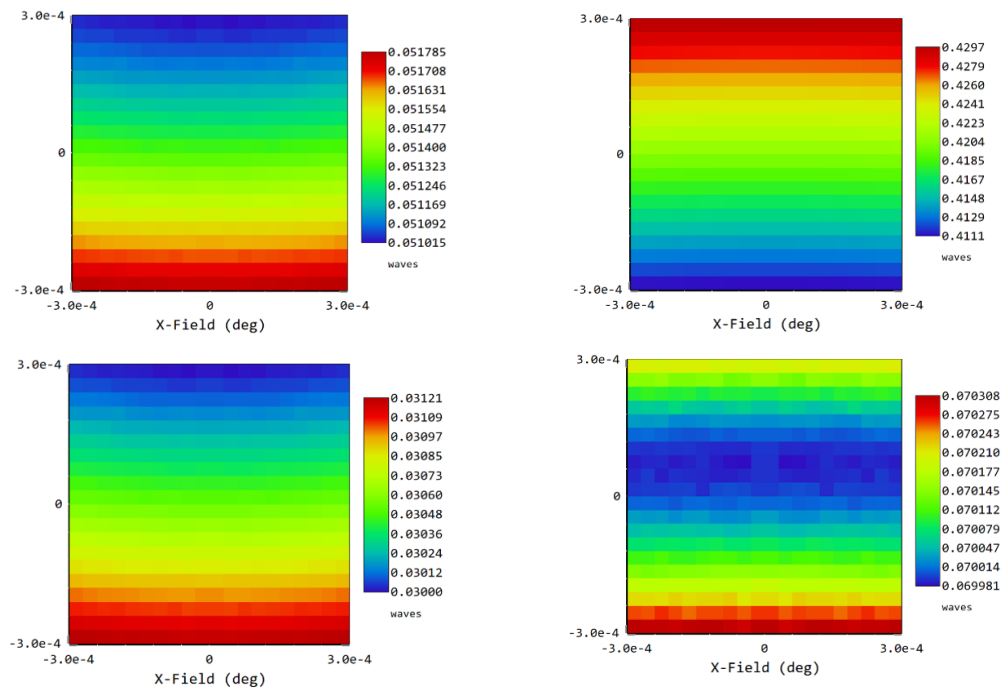


Figure 20. Comparison between maps of the LGS rms WFE over a 3'' FoV at 104 km: new design (left) and preliminary design (right), polychromatic (top) and monochromatic (bottom).

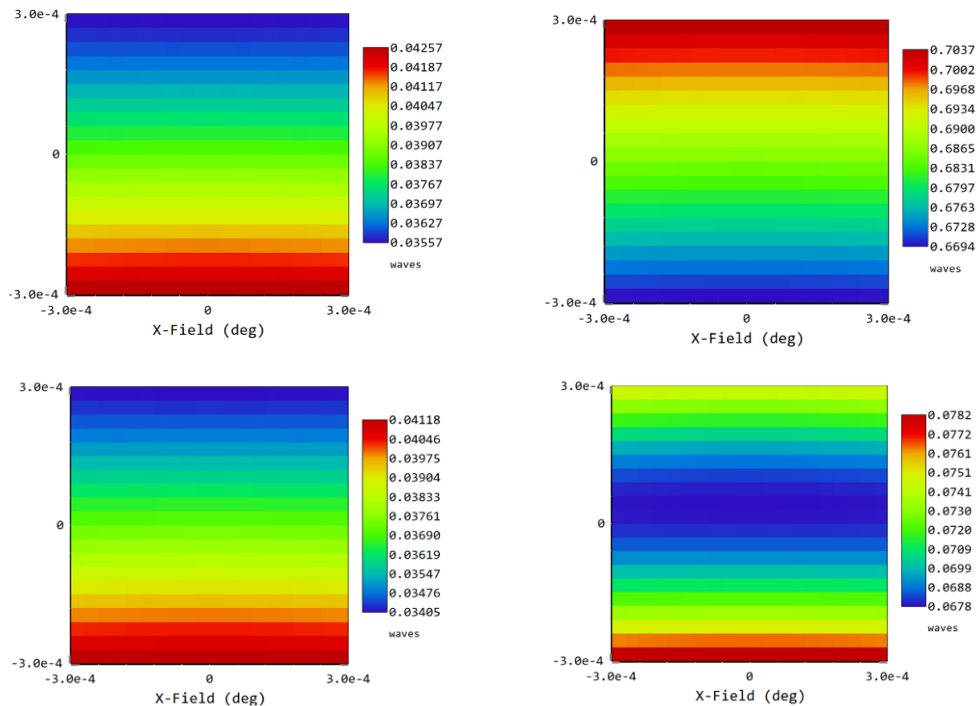


Figure 21. Comparison between maps of the LGS rms WFE over a 2''x2'' FoV at 150 km: new design (left) and preliminary design (right), polychromatic (top) and monochromatic (bottom).

5.1.3 Summary

All the previous analyses can be summarized by a single, average, value of WFE, computed for each PUA optical configuration and reported in Table 2.

For each configuration different field positions and wavelengths have been defined:

- For NGS-REF and NGS-LO, the technical FoV is sampled over 17 different positions, each with a unit weight (except for those at the edge of the FoV, i.e. at 80'', with a weight of 0.2), and the WFE is averaged over three wavelengths (the central one plus the two at the edge of the band, all with unit weight).
- For NGS-MIC, a 3x3 regular grid within the 53''x53'' MICADO FoV is defined, and the WFE averaged over three wavelengths (the central one plus the two at the edge of the band, all with unit weight).
- For LGS, 3'' sources are simulated, with 4 fields at 45'' radial distance from the center, plus 4 fields at 43.5'' and 4 at 46.5'', and the WFE averaged over three wavelengths (the central one plus the two at the edge of the band, all with unit weight).

Table 2. Performance of the new PUA optical layout: nominal WFE (nm, rms), averaged as described in the text, computed at the central wavelength (nm) of the band defined for each group of sources. The maximum allowed WFE is reported for an immediate comparison.



	NGS-REF	NGS-LO	NGS-MIC	LGS@104km	LGS@150km
Central wavelength	800	1650	1650	589	589
Nominal design WFE, nm rms	21	22	13	30	23
Max WFE, nm rms (spec)	60	150	60	100	100

5.2 WFE budget

One of the main goals of this revision process is also to check the self-consistency of the given WFE budget, its allocation to different error sources, and to derive proper optical tolerances that need to be met in order to guarantee the final WFE performances.

The next subsection (5.2.1) describes the general approach; all numerical data and results are reported in RD1.

5.2.1 Sensitivity analysis

To build a reliable WFE budget, a sensitivity analysis has been carried out for each main configuration: the results are reported in RD1. The WFE is a weighted average over the field and over the waveband, as described in Section 5.1.3.

Tolerances have been split into three main subsets:

- *Optical manufacturing*: all tolerances defined at optical component level that will drive their manufacture. These will be part of the specifications (according to ISO 10110 standards) assigned to optical components, like the radius of curvature, material index of refraction and homogeneity, center thickness, centration, surface irregularity. Other optical specifications, such as the surface micro-roughness, that do not directly affect the WFE budget are not considered here.
- *Assembly, Integration and Environment*: these are the tolerances to be allocated during the assembly and integration phases of the single optical components inside their opto-mechanical mounts, before alignment. For example, any distortion induced by the mount will be part of this budget. Moreover, environmental effects, such as gravity and temperature, will flow inside this budget, being related mostly to the mechanical mount definition and will help to drive the definition of the mechanical mount specifications.
- *Alignment and Verification*: this relates to the alignment (rigid-body) errors of optical components, and those errors related to the measurement errors coming from optical and/or mechanical metrology. Not all optical components will have adjustments to compensate for integration errors. Moreover, not all 6 degrees of freedom will need to be adjusted. The goal of the alignment procedures is to define the minimal set of adjustments capable of achieving optimal alignment. Many optical components or subsystems will be placed in position within mechanical tolerances,



without any adjustment, to simplify the overall alignment of the PUA: this translates into time and cost savings, enhances reproducibility, and improves the reliability of the system performances.

Optical manufacturing

Errors in this category are:

- Material refractive index: mostly affecting lenses. All the PUA optics with the exception of CBS and LGS lenses, are made of Fused Silica (the CBS will likely be made of Fused Silica, as well, but the final material choice shall be further investigated). Fused Silica is a very pure material, with very small variations in refractive index. The LGS lenses will be made of other optical glasses, and some tolerances are required to be assigned to the (average) refractive index, generally defined by the refractive index at a reference wavelength, and its wavelength dependence as defined by the Abbe number at that reference wavelength.
- Material homogeneity: this is related to the spatial variation of the refractive index inside the bulk of the optical components. This affects the static WFE. While most optical components will induce small errors, the bulky CBS will likely induce a quite large error. Some compensation strategies have been already identified.
- Radius of curvature: the error in the nominal radius will affect powered optics. Air spacing is generally used to compensate for these errors.
- Center thickness: typical manufacturing errors for this kind of precision optics are in the 0.1%-0.3% regime.
- Wedge angle: some optics, namely the two BS1 and BS2 beam-splitters, have a non-zero wedge angle. All other plano optics will have zero nominal wedge angles. However, in both cases, some residual wedge error will be present, introducing some aberrations, mostly lateral color or astigmatism.
- Centration: lenses and aspherical components will be affected by centration errors. Sensitivities have been derived. All spherical lenses will be centered during the integration and alignment procedures, to fully compensate for their centration errors. The only residual errors that cannot be fully corrected are due to the aspherical components (of D1, PM and EM). Centration errors on mirrors will be fully compensated during the optical alignment.
- Surface irregularity: this is the main manufacturing error considered in the WFE budget. In fact, due to the high number of optical components and surfaces, such errors dominate the overall WFE budget.

Integration and Environment

The Integration and Environment are the two main areas to be taken into account while designing and building the PUA, mostly related to the opto-mechanical system, its interfaces to the optical components, and their performances.

- Integration: here are collected all the errors induced by the integration processes of the optical components into their own mounts, such as misplacement of the component inside the holder, or wrong momenta applied by the mount itself. Another error source is the wrong position of those elements that do not have adjustments



to align the optics along the nominal optical path. Other errors can be the result of the subsystem and system level integration steps, when they are not cinematically decoupled.

- **Environmental effects:** this encompasses those effects due to the gravity deformation of the optical components while in operation, and the effects that arise from variations in the ambient temperature or pressure. It may include displacement of optical components due to transport load conditions, if they are not dismounted, and loads from earthquakes. At this stage, only allocations have been defined, because a detailed mechanical and thermal modeling is required to verify these types of effects.

Alignment and Verification

Here we group together the residual errors while aligning the optics and test optical performance.

- **Optical Alignment** (described in Section 5.6): its main purpose is to compensate for all the unavoidable small errors during all the previous phases, including manufacturing, assembly, and integration. By careful selection of the adjusting degrees of freedom (DoF), it is possible to reduce the overall system WFE, thus improving the performance of the PUA. In this budget we include all the residual alignment errors of those adjusting DoF.
- **Metrology:** the auxiliary systems used to align and verify the optical performance of the PUA will also have their own errors, related to their accuracy and repeatability. Both effects need to be considered here. For example, while using reference optics like an accurate plano mirror to close an interferometric cavity, some errors are associated with the reference optical surface. The long optical path of the PUA also gives rise to errors while acquiring the wavefront, due to vibration and air turbulence. While these effects can be minimized by averaging and clever control of the test environment, there are still some residual errors. Some of them are random in nature, affecting the repeatability of the measurement, while others, like air thermal gradients, are systematic errors, more difficult to remove or calibrate out.

5.2.2 Tolerance analysis (MonteCarlo)

All the tolerance ranges used for the MonteCarlo analyses are collected in Table 3.

Table 3. Summary of all the optical parameters and relative tolerances considered in the analyses. Fringe tolerances, used to simulate flat optics curvature, are referred to a wavelength of 0.8 μm .

Type	Parameter	Optics	Tolerance range		Unit	Notes
Positioning	Despace Z	All	-0.2	0.2	mm	
	Decenter X	PM, EM	-0.1	0.1	mm	



		CBS, LFM, BS2	-0.2	0.2	mm	
		SM	-0.3	0.3	mm	
		L1, D1, D2	-0.03	0.03	mm	
		W, BS1	-0.5	0.5	mm	
	Decenter Y	PM, EM	-0.1	0.1	mm	
		CBS, LFM, BS2	-0.2	0.2	mm	
		SM	-0.3	0.3	mm	
		L1, D1, D2	-0.03	0.03	mm	
		W, BS1	-0.5	0.5	mm	
	Tip θ_x	W, SM	-0.002	0.002	deg	
		BS2	-0.02	0.02	deg	
		All others	-0.01	0.01	deg	
	Tilt θ_y	W, SM	-0.002	0.002	deg	
		BS2	-0.02	0.02	deg	
		All others	-0.01	0.01	deg	
	Rotation θ_z	All	-0.05	0.05	deg	
Manufacturing – Surface flatness	See Table 5					
Manufacturing – All others	Thickness	All	-0.2	0.2	mm	
	Coaxiality	(Centering) L1, D1, D2	-50	50	um	
		(Angle) L1, D1, D2	-30	30	arcsec	
	Wedge	W, CBS, BS1, BS2	-30	30	arcsec	
	Radius of Curvature	SM, EM	-0.05	-0.05	%	
		All others	-0.1	0.1	%	
	Conic constant	EM	-1%	1%	-	
	Fringe	CBS-diag	-0.25	0.25	-	
		CBS-sides	-0.5	0.5	-	
		PM, BS1, BS2, LFM	-0.5	0.5	-	
		W	-1	1	-	
	Glass	Refraction Index	-0.03	0.03	%	All
		Abbe Number	-0.3	0.3	%	All

Alignment

A statistical analysis has been performed to check the effects of the alignment errors in terms of induced WFE and the effectiveness of the main system compensators.

A dedicated *Zemax* model has been built for each configuration, where the tolerance ranges defined in Table 3 and RD1 have been introduced, and the following compensators have been considered:

- NGS configurations: Mask focus, decenter X, decenter Y, tilt X, tilt Y;
- LGS configurations: Distance D1-D2 (focus), LGS arm decenter X, decenter Y, tilt X, tilt Y.



The retrieved WFE values are weighted averages over the field and over the waveband, as described in Section 5.1.3. For each configuration a MonteCarlo analysis with 100 runs (the analysis with compensators is quite demanding from a computational point of view) and parabolic statistics has been carried out.

The results of the analyses are summarized in Table 4, in terms of induced WFE (a parabolic statistics and a coverage of 90% have been considered).

Table 4. Induced WFE (nm, rms) due to alignment tolerances. Runs: 100. Statistics: parabolic. Coverage: 90%.

NGS-REF (800 nm)	NGS-MIC (1650 nm)	LGS@104km (589 nm)	LGS@150km (589 nm)
9	7	11	11

Surface irregularities

A statistical analysis has been performed to check the effects of the irregularities of the optical surfaces in terms of induced WFE, since those contributions dominate the overall budget.

A dedicated *Zemax* model has been built for each configuration, where the tolerance ranges defined in RD1 have been introduced through TEZI operands (able to model random surface shapes combining standard Zernike – in *Noll* notation – coefficients to obtain a certain rms value of surface sag within the defined tolerances). These ranges have been allocated for the Zernike terms from 5 to 11, while for the Zernike terms from 12 to 36 additional tolerance ranges have been defined (not reported in RD1) and a dedicated analysis has been performed.

The retrieved WFE values are weighted averages over the field and over the waveband, as described in Section 5.1.3. For each configuration and class of irregularities a Monte Carlo analysis with 500 runs and uniform statistics has been carried out.

The tolerance values are reported in Table 5, and the results of the analyses are summarized in Table 6.

Table 5. Surface irregularity values defined for the PUA optical elements (surface naming in agreement with RD3).

Optical element	Surface #	Irregularity Z5-Z11 (nm, rms)	Irregularity Z12-Z37 (nm, rms)
W	W-S1	20	6
	W-S2	10	5
SM	SM-S1	10	5
	SM-S2	20	10
CBS	all	10	5
PM	-	5	4
BS1	BS1-S1	20	10



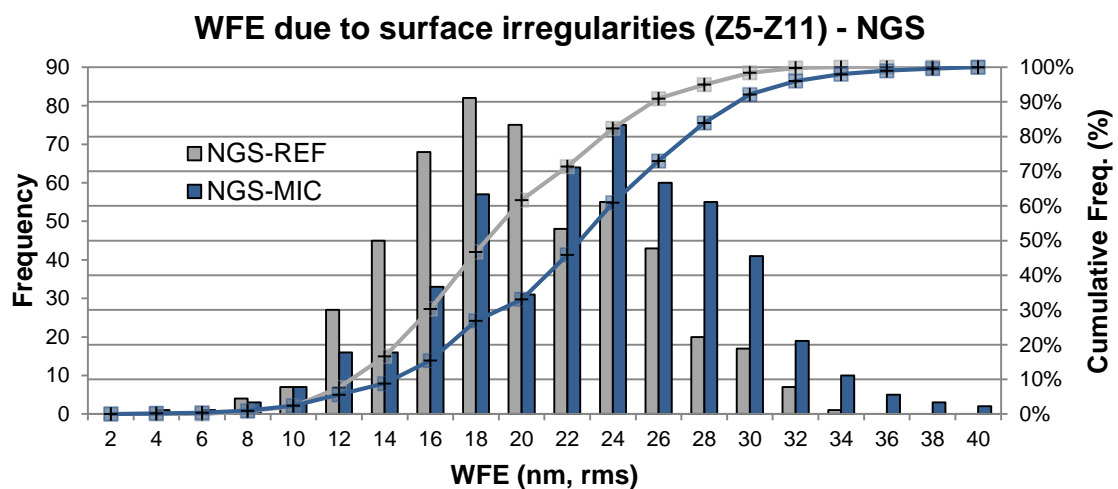
	BS1-S2	10	5
BS2	BS2-S1	10	5
	BS2-S2	20	10
EM	-	10	5
L1	all	10	5
LFM	-	10	5
D1	all	20	10
D2	all	20	10

Table 6. Induced WFE (nm, rms) due to surface irregularities tolerances. Runs: 500. Statistics: uniform. Coverage: 90%.

	NGS-REF (800 nm)	NGS-MIC (1650 nm)	LGS@104km (589 nm)	LGS@150km (589 nm)
Z5-Z11	26	29	35	32
Z12-Z37	17	17	22	20
TOT (RSS)	31	34	42	37

The results, reported in Table 9, are in good agreement with what is estimated in RD1. It is finally worth underlining that the computed values of WFE are conservative, because a high statistical coverage (90%) has been considered and no compensator has been taken into account.

As an example, we finally report histograms of the tolerance analysis results for Zernike modes up to Z11.



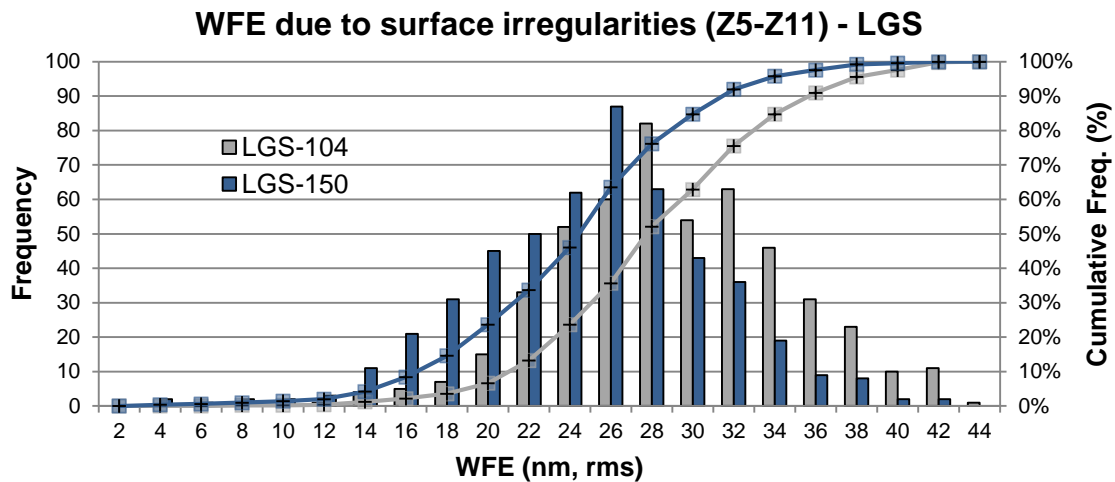


Figure 22. Results of the tolerance analyses (Montecarlo) for Zernike modes up to Z11: NGS WFE (top), LGS WFE (bottom). 500 runs, uniform statistics, no compensators.

Other manufacturing tolerances

A statistical analysis has been performed to check the effects of the other manufacturing errors in terms of induced WFE and the effectiveness of the main system compensators. A dedicated *Zemax* model has been built for each configuration, where the tolerance ranges defined in RD1 and Table 3 have been introduced, and the following compensators have been considered:

- NGS configurations: Mask focus, decenter X, decenter Y, tilt X, tilt Y;
- LGS configurations: Distance D1-D2 (focus), Distance W-SM.

The retrieved WFE values are weighted averages over the field and over the waveband, as described in Section 5.1.3. For each configuration a MonteCarlo analysis with 100 runs (the analysis with compensators is very demanding from a computational point of view) and uniform statistics has been carried out.

The results of the analyses are summarized in Table 7, in terms of induced WFE (a uniform statistics and a coverage of 90% have been considered).

Table 7. Results of the tolerance analyses on the manufacturing tolerances (no surface irregularities): induced WFE (nm, rms). Runs: 100. Statistics: uniform. Coverage: 90%.

NGS-REF (800 nm)	NGS-MIC (1650 nm)	LGS@104km (589 nm)	LGS@150km (589 nm)
20	30	32	28



5.2.3 Thermal aspects

The tight WFE budget and the quite large operating range of temperature (0°C-15°C) would impose the dynamic adjustment of the PUA focal planes. This comes for free only for the LGS path, where a high-precision linear stage moves the focal plane with the LGS sources at the proper position, according to the selected conjugation altitude.

The provision of a motorized DoF for the NGS mask piston (to dynamically control and adjust the mask focal position according to the measured temperature) can be avoided in case of re-focusing at MORFEO level: the possibility to compensate through a piston of MORFEO DM2 (MM10) has been considered as baseline. The values of maximum re-focusing distance are reported in Table 8.

Table 8. Values of re-focusing distance computed considering a reference temperature of 9°C and an operating range of temperature from 0°C to 15°C (signs according to Zemax model convention).

ΔT	Re-focusing distance (mm)		
	PUA – NGS mask piston	MORFEO – NGS focal plane	MORFEO – DM piston
-9°C	0.068	-1.009	-0.514
+6°C	-0.038	0.512	0.262

5.2.4 WFE breakdown

All the sensitivity analyses and error allocations reported in section 5.2.1 have been collected in RD1. Optical tolerances have been assigned to each effect, whenever possible. When analysis was deemed not possible, proper values based on past experience have been applied, and a reasonable value allocated in the budget.

Table 9 summarizes all the WFE contributions. The overall results indicate that some WFE compensation strategy will likely be required to meet the tight NGS WFE requirements. The compensation strategy, clearly identified and described in Section 5.2.5, is considered as a design baseline, therefore the final compliance shall be verified with regards to the compensated values of WFE (these values will be refined to balance NGS and LGS performance by applying partial compensation as needed).

It is worth remarking that we will provide this WFE breakdown to the contractor as a reference. The contractor will be free to allocate contributions in a different way, provided that the specifications on the total WFE are met.

Table 9. WFE preliminary breakdown for the new PUA design.



#	Type	Description	Wavefront error - Field averaged - Polychromatic				
			Units: nm RMS				
			LGS @104km 589 nm	LGS @150km 589 nm	NGS-REF 800 nm	NGS-LO 1650 nm	NGS-MIC 1650 nm
1	Design		29	22	21	22	16
1,1		Nominal aberrations	29	22	21	22	16
2	Optical manufacturing		56	53	47	50	49
2,1		Material homogeneity	33	32	32	32	32
2,2		Radius of curvature (telescope)	2	2	2	2	2
2,3		Radius of curvature (ellipt.)			4	4	3
2,4		Radius of curvature (LGS lenses)	12	17			
2,5		Thickness	7	2	7	7	7
2,6		Wedge	6	6	15	15	13
2,7		Centration	8	9	0	0	0
2,8		Surface irregularity	42	37	31	34	34
2,9		Refractive index & Abbe	3	3	0	0	0
3	Integration		28	28	18	18	18
3,1		Clamping forces & moments	28	28	9	9	9
3,2		LGS translation stage	2	2			
3,3		NGS mask curvature & fibres			15	15	15
4	Optical alignment		14	13	10	10	10
4,1		CU "telescope" (W+SM)	7	6	3	3	3
4,2		NGS optics			9	9	9
4,3		LGS optics	13	12			
5	Gravity		23	21	12	12	12
5,1		Gravity induced (static, compensated)	23	21	12	12	12
6	Environment		18	18	18	18	18
6,1		Isothermal change (incl. defocus)	10	10	10	10	10
6,2		Horizontal gradients	10	10	10	10	10
6,3		Vertical gradients	10	10	10	10	10
6,4		Air pressure	5	5	5	5	5
7	Metrology		17	17	17	17	17
7,1		Test repeatability	10	10	10	10	10
7,2		Reference surfaces	10	10	10	10	10
7,3		OGSE	10	10	10	10	10
		TOTAL (RSS)	78	73	62	64	62
8	Compensation						
		REQUIREMENT	100	100	60	150	60
		Margin	62	69		136	

5.2.5 WFE compensation strategy

Despite all the efforts during the design and AIV phases, and also related to some large uncertainties for some specific error sources such as the blanks' homogeneity, it might be possible that some WFE performance will not be met. For this reason, it is highly recommended to identify some recovery actions, such as working on some optical components to compensate for residual errors (backup strategy successfully proved in other projects).

This technique can be used to compensate for field-invariant aberrations, when present, by adding a correction map at one of the pupil planes of the system. The PUA offers such a possibility, because it provides a natural position for such a correction optics, that is the Pupil Mirror (PM), or the Deformable Mirror (DM) in TU configuration. This is likely to be quite effective, because we expect that a large fraction of the overall system WFE will come from the CBS and this component is very close to the aperture stop of the optical system. Then, by measuring the WFE across the field for the different configurations, it is possible to derive the shape of the correction map that will (at least partially) compensate for the measured WFE.

The foreseen procedure is the following:



- PUA is integrated and the WFE is measured over the NGS and LGS arms at different field positions (on-axis, off-axis);
- The field average WFE is computed, by using, for example, a polynomial representation such as the first 36 Zernike modes;
- The PM (or a spare one) shape will be figured, summing together the nominal aspherical profile of the PM and the correction map;
- The PM is installed back in the PUA and WFE is tested again.

In Test Unit configuration, there is no need to rework the PM, because there will be the possibility to apply the correction map directly on the DM. Indeed, if a DM will be available in advance while integrating and testing the PUA, it will prove to be very effective to test this strategy even before applying a permanent correction map on the PM.

The effectiveness of this mitigation strategy has been proven through the analysis described below.

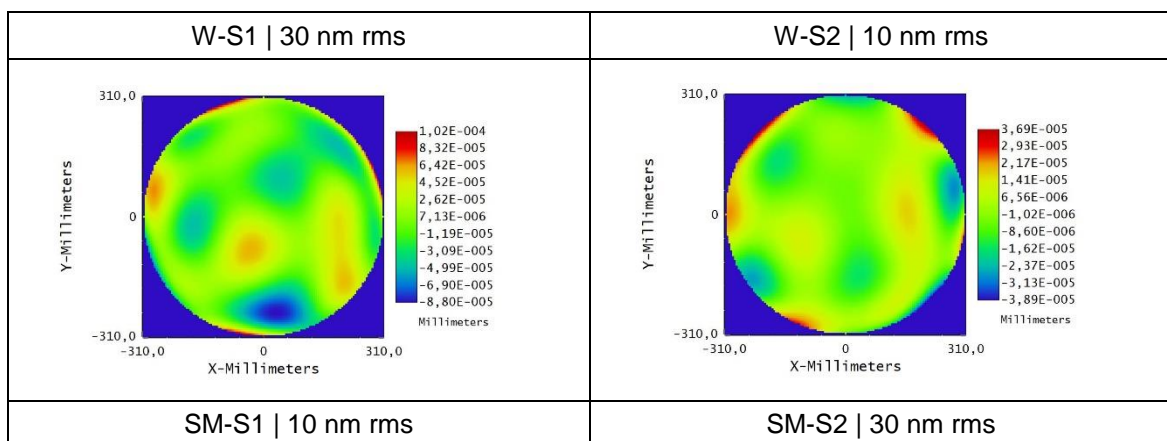
A proper *Zemax* model with NGS-REF and NGS-MIC nominal configurations has been built, where surface irregularities and blank in-homogeneities have been considered and implemented:

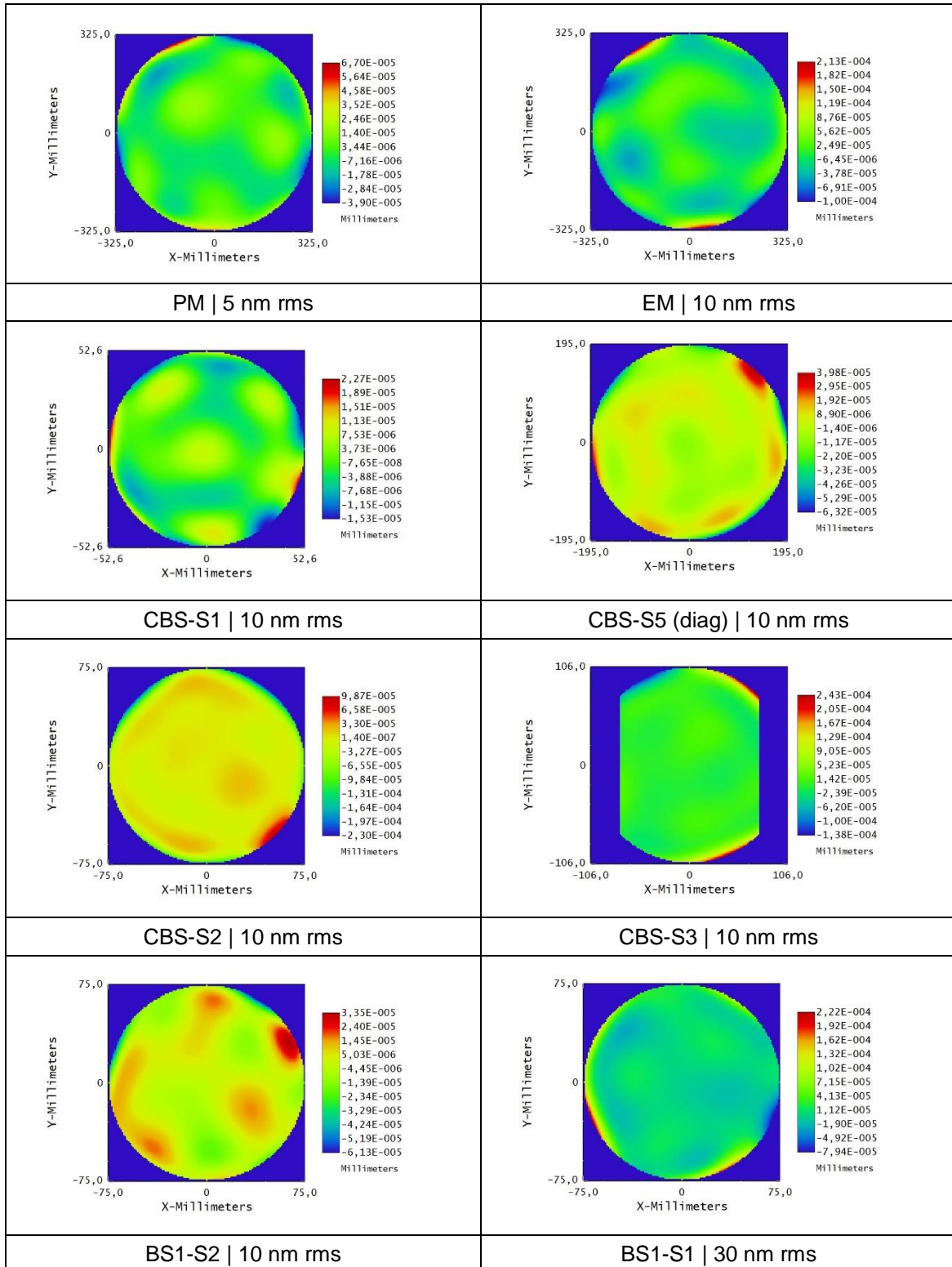
- Surface irregularities are described through Zernike standard sag coefficients, produced randomly according to the tolerance interval defined for each element;
- Glass inhomogeneities are described through Zernike fringe phase coefficients, randomly produced starting from a real phase map provided by *Heraeus* and properly scaled according to the homogeneity level defined for each optical component and to the central wavelength of the optical configuration under evaluation.

Although the main goal of the compensation strategy is to reduce the effect of glass inhomogeneities, it has been decided to also include the surface irregularities in the model because both will be present and merged in the measure of the PUA WFE (that will eventually drive the PM final polishing).

The worst of 100 MonteCarlo runs has been considered as the reference model (simulated surfaces in Table 10) and in this model the effects of glass inhomogeneities (simulated surfaces in Table 11) have been implemented.

Table 10. Compensation strategy reference model: maps of surface irregularities/sags (Z5-Z36).





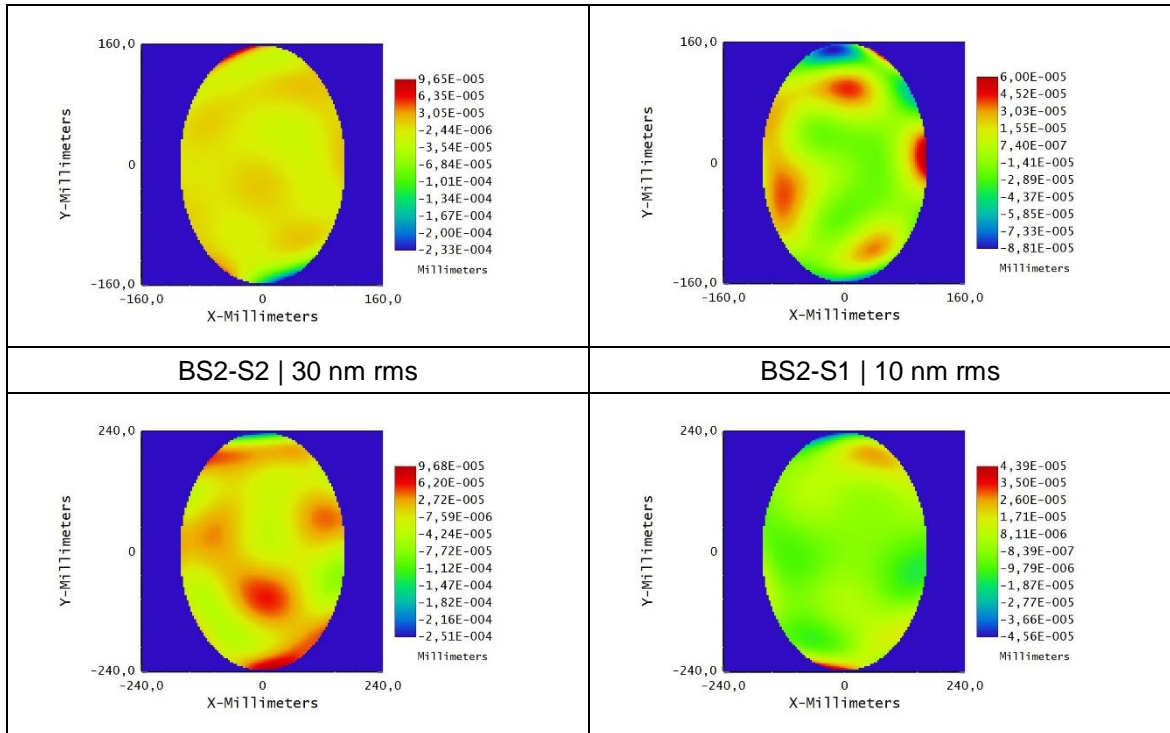
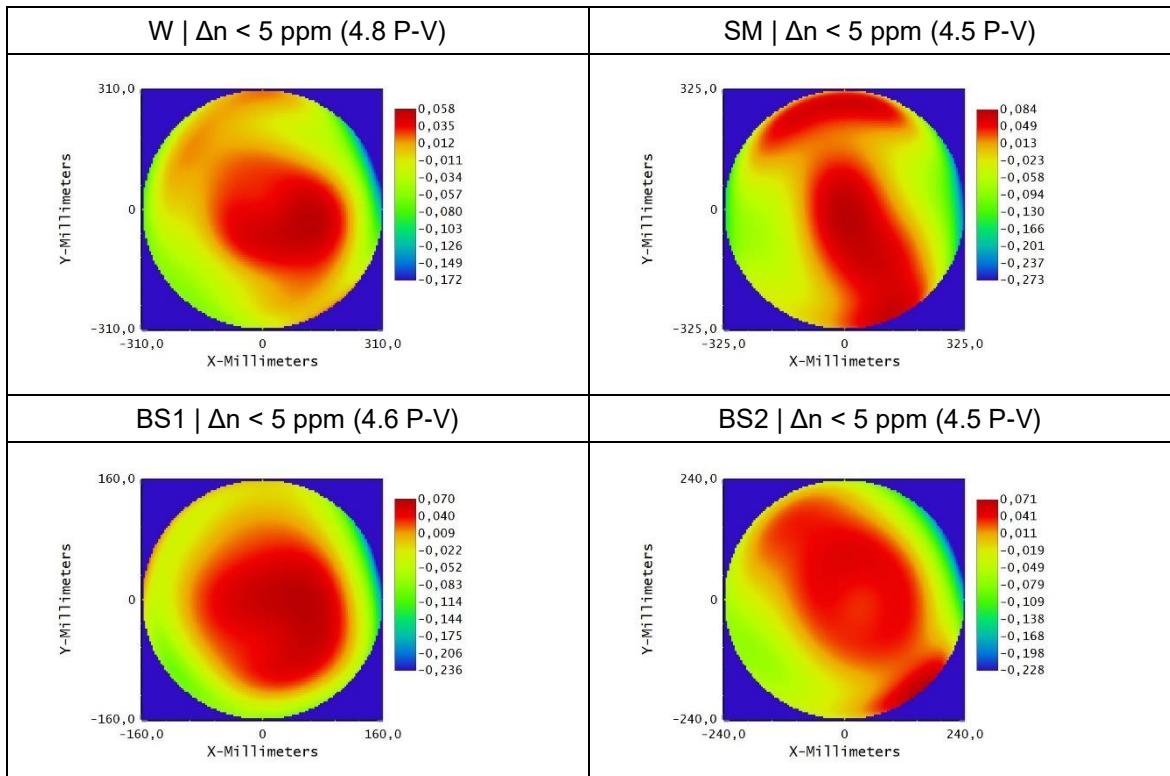
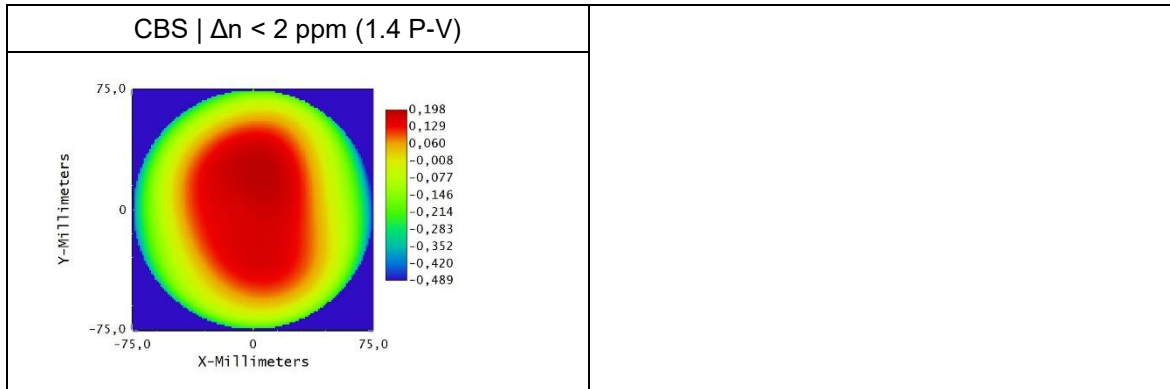


Table 11. Compensation strategy reference model: phase maps of glass homogeneities (Z4-Z36) @800nm.





Results and compensation (NGS)

The simulated surface sag maps (surface irregularities) in the reference model introduce the following net WFE (rms), after re-focusing:

- 35 nm for NGS-REF
- 33 nm for NGS-MIC.

The simulated surface phase maps (inhomogeneities) in the reference model introduce the following net WFE (rms) after re-focusing:

- 39 nm for NGS-REF
- 41 nm for NGS-MIC.

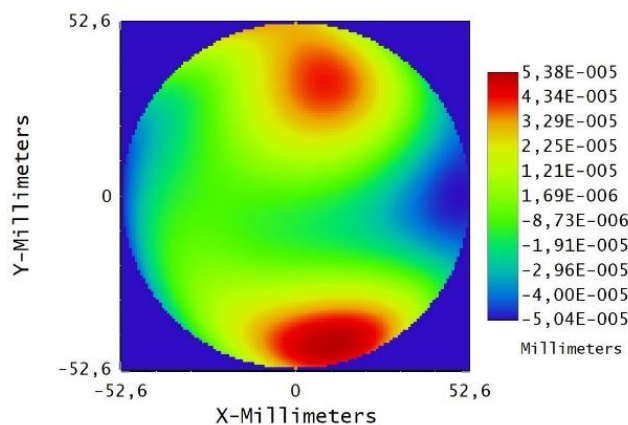
When uncompensated, the total WFE (nominal + surface irregularities + glass inhomogeneities) in the reference model is:

- 56 nm for NGS-REF
- 55 nm for NGS-MIC.

There is little/no margin for other WFE sources.

A large WFE reduction (~50 nm) is achievable by applying on the PM the compensation map shown in Figure 23, reducing the total WFE down to the following residual values:

- 15 nm for NGS-REF
- 19 nm for NGS-MIC.



Zernike #	Sag value (nm)
Z5	-
Z6	-21
Z7	-5
Z8	2
Z9	-
Z10	-6
Z11	-4
Z12	4
Z13	-4
Z14	-
Z15	2
Z16	-
Z17	4
Z18	3

PV = 104 nm | RMS = 21 nm



Figure 23. Optimal compensation map to apply to the PM to minimize the model NGS WFE.

Consequences (LGS)

The PM compensation map is computed to optimize the NGS performance, but this leads to a worse LGS performance, as expected.

Considering the reference model (worst of 100 MC for NGS) with the LGS nominal arm downstream, the simulated surface sag maps (surface irregularities) plus the simulated surface phase maps (in-homogeneities) introduce the following net WFE (rms), after re-focusing:

- 39 nm for LGS-104km
- 27 nm for LGS-150km

When the PM compensation map is included in this model, the total WFE (rms) is:

- 77 nm for LGS-104km
- 64 nm for LGS-150km

It is thus possible to estimate the net WFE (rms) contribution of the PM compensation map on the LGS WFE budget: ~50 nm.

Finally, if one puts this last WFE contribution in the LGS WFE breakdown (Table 9), the total WFE increases to ~90 nm.

The WFE values obtained from the simulation just described are summarized in Table 12.

Table 12. Summary of the results of the simulation. “COMP” identifies the presence of the PM compensation map (optimized for NGS).

WFE (nm rms)	NGS-REF (800 nm)	NGS-MIC (1650 nm)	LGS-104km (589 nm)	LGS-150km (589 nm)
Nominal	21	13	30	23
Nominal + Surface irr.	41	36	47	41
Nominal + Surface irr. + Glass homog.	56	55	51	37
Nominal + Surface irr. + Glass homog. + COMP	15	19	~90	~90

Comments

- 1) The chosen reference model is pessimistic. It represents a situation which is very likely worse than what would be obtained in reality, for two main reasons:
 - a) The chosen run is the worst of 100 runs for the NGS optical path.
 - b) For simplicity, for the CBS we have considered a single ‘average’ value of homogeneity (1.4 ppm P-V) for the whole optical path (300 mm), while in reality the manufacturer will very likely provide a lower level in the main direction of beam propagation.



- 2) In order to obtain a consistent WFE evaluation, the phase maps for the NGS-MIC configuration have been scaled for a factor 0.485 with respect to the same of the NGS-REF configuration, because the ratio of the two central wavelengths (800/1650) is precisely 0.485. Similarly, the phase maps for LGSs have been scaled for a factor 1.358 (800/589).

Conclusions

- 1) The results of the simulation show the effectiveness of the compensation strategy based on a final polishing of the PM, identified as a risk mitigation strategy in case the NGS WFE measured after the alignment exceeds the requirement.
- 2) The definition of the optimal shape of the PM should also take into account the need to limit the unavoidable worsening of the LGS performance (trade-off).
- 3) The compensation strategy is considered as a design baseline, therefore the final compliance shall be verified with regards to the compensated values of WFE (these values will be refined to balance NGS and LGS performance by applying partial compensation as needed).

5.3 Pupil quality

The pupil quality has been evaluated in terms of pupil blur, distortion, shift and position. It must be emphasized that the optical components that control the pupil quality are only those between the aperture stop at the intermediate pupil plane and the exit pupil plane, namely the part of the CBS in reflection (second pass of the optical beam), the spherical mirror SM and the window W. The CUFM, placed in front of the MORFEO entrance focal plane, will also play a role, albeit a minor one, as it is closer to the focal planes. Figure 24 shows the spot diagrams projected at the PUA exit pupil plane, coincident with both the ELT exit pupil and the MORFEO entrance pupil plane, for point source objects placed at the PUA internal pupil plane (PM surface). Even in the worst case, corresponding to the pupil edges and the shortest wavelength, the image rms blur is well below 1% of the pupil diameter (~0.5%). Figure 25 shows the plot of geometrical distortion introduced by the PUA optics on the output pupil plane, with a maximum value of ~0.03%. For what concerns the PUA exit pupil position and shift, these are influenced by the mutual position of W and SM, in terms of distance, decenter and tilts.

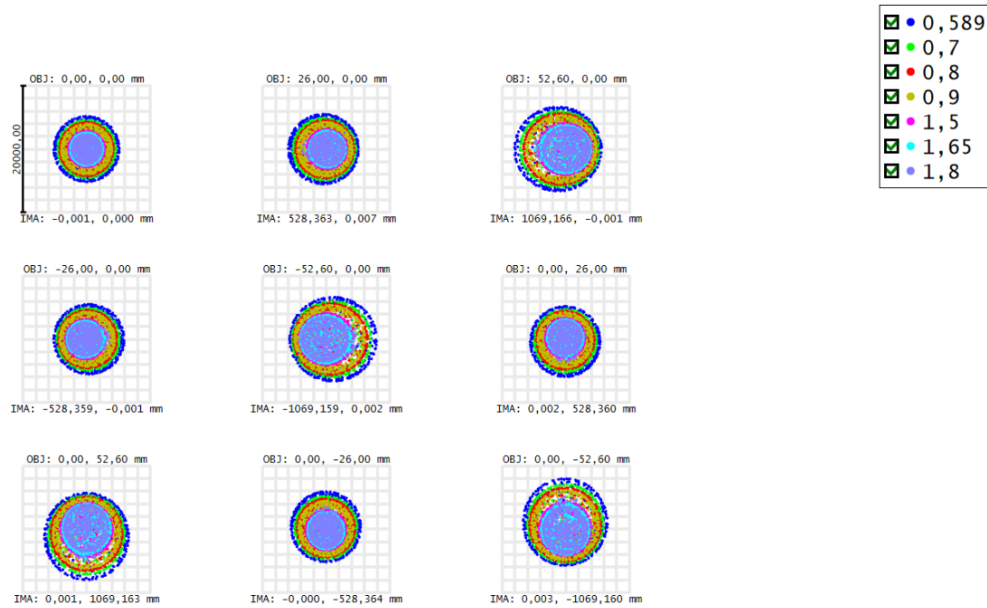


Figure 24. Performance of the new PUA optical layout: pupil blur at different pupil positions and all the PUA wavelengths.

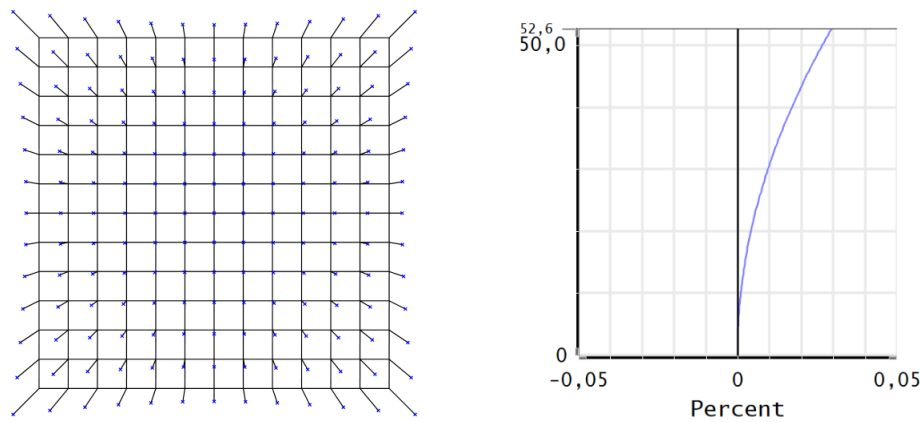


Figure 25. Performance of the new PUA optical layout: pupil distortion grid (left) and plot (right, %).

5.3.1 Tolerance analysis

Tolerance analyses have been performed to check the adequacy of the set of tolerances defined for WFE purposes (RD1 and Table 3). The full list of operands and tolerance values is reported in Table 13, the results are summarized in Table 14, Table 15 and Table 16.

Assumptions:

- The optical components that control the pupil quality are the ones placed “after” the PUA pupil stop: half CBS, SM, W and CUFM.



- The tolerance operands associated with system DoFs identified as compensators for the system (alignment purposes) are not included in the simulation (i.e. CUFM tip/tilt for PUA-MORFEO mutual alignment, PM tip/tilt for PUA internal alignment).
- The CUFM positioning DoFs are not included in the simulation (for the reason above), while the CUFM manufacturing tolerances are (however they play a marginal role).
- No compensators have been considered in the MC simulations.
- Merit Function: RMS Spot Radius in mm (sampling: 10 | Fields: XY symmetric).
- 500 MonteCarlo runs, uniform statistics, 90% coverage.

Table 13. List of tolerance operands and values used for pupil quality tolerance analyses.

Type	Surf	Adjust	Nominal	Min	Max	Comment
TOFF ▼						AIV
TOFF ▼						Distances
TTHI ▼	24	24	970,000	-0,200	0,200	CUFM-W
TTHI ▼	13	13	670,000	-0,200	0,200	W-SM
TTHI ▼	10	10	275,327	-0,200	0,200	SM-CBS
TTHI ▼	2	2	-10,000	-0,200	0,200	CBS-Pup
TOFF ▼						W
TPAR ▼	15	1	0,000	-0,200	0,200	decx
TPAR ▼	15	2	0,000	-0,200	0,200	decy
TPAR ▼	15	3	0,000	-1,000E-02	1,000E-02	tip
TPAR ▼	15	4	0,000	-1,000E-02	1,000E-02	tilt
TOFF ▼						SM
TPAR ▼	11	1	0,000	-0,200	0,200	decx
TPAR ▼	11	2	0,000	-0,200	0,200	decy
TPAR ▼	11	3	0,000	-1,000E-02	1,000E-02	tip
TPAR ▼	11	4	0,000	-1,000E-02	1,000E-02	tilt
TOFF ▼						CBS
TPAR ▼	3	1	0,000	-0,200	0,200	decx
TPAR ▼	3	2	0,000	-0,200	0,200	decy
TPAR ▼	3	3	0,000	-1,000E-02	1,000E-02	tip
TPAR ▼	3	4	0,000	-1,000E-02	1,000E-02	tilt



TOFF ▾						MANUF
TOFF ▾						Glass
TIND ▾	22			1,458	-3,000E-04	3,000E-04 W
TIND ▾	12			1,458	-3,000E-04	3,000E-04 SM
TIND ▾	4			1,517	-3,000E-04	3,000E-04 CBS
TIND ▾	8			1,517	-3,000E-04	3,000E-04 CBS
TABB ▾	22			67,821	-0,200	0,200 W
TABB ▾	12			67,821	-0,200	0,200 SM
TABB ▾	4			64,167	-0,200	0,200 CBS
TABB ▾	8			64,167	-0,200	0,200 CBS
TOFF ▾						CUFM
TFRN ▾	28			0,000	-1,000	1,000
TOFF ▾						W
TFRN ▾	22			0,000	-1,000	1,000 W low
TFRN ▾	24			0,000	-1,000	1,000 W up
TPAR ▾	23	3		0,000	-8,500E-03	8,500E-03 30" parall
TPAR ▾	23	4		0,000	-8,500E-03	8,500E-03 30" parall
TTHI ▾	22	22		30,000	-0,200	0,200 W thick
TOFF ▾						SM
TRAD ▾	12	0		3700,000	-2,000	2,000 0.05% RoC
TRAD ▾	13	0		3700,000	-2,000	2,000 0.05% RoC
TTHI ▾	12	12		50,000	-0,200	0,200 SM thick
TOFF ▾						CBS
TFRN ▾	4			0,000	-0,500	0,500 flatness
TFRN ▾	6			0,000	-0,250	0,250 flatness
TFRN ▾	10			0,000	-0,500	0,500 flatness
TPAR ▾	5	3		-45,000	-1,000E-02	1,000E-02 Prism angle tol 36"

TOFF ▾						FLATNESS
TOFF ▾						Zern up to 37
TEZI ▾	28	37	5	0,000	-3,000E-05	3,000E-05 CUFM
TEZI ▾	24	37	5	0,000	-3,000E-05	3,000E-05 W up
TEZI ▾	16	37	5	0,000	-1,000E-05	1,000E-05 W low
TEZI ▾	13	37	5	0,000	-1,000E-05	1,000E-05 SM up
TEZI ▾	12	37	5	0,000	-3,000E-05	3,000E-05 SM low
TEZI ▾	4	37	5	0,000	-1,000E-05	1,000E-05 CBS side
TEZI ▾	6	37	5	0,000	-1,000E-05	1,000E-05 CBS diag
TEZI ▾	10	37	5	0,000	-1,000E-05	1,000E-05 CBS side

Blur

Surface flatness tolerances are not significant offenders for the blur.

Worst offenders:

1. SM RoC tolerance (+2 mm) – this is the worst offender
2. Distance W-SM (-0.2 mm)
3. Distance Pupil-CBS (-0.2 mm)
4. Distance CBS-SM (-0.2 mm)
5. SM thickness (-0.2 mm)

Table 14. Pupil quality tolerance analysis summary: pupil blur. The computed max blur (the blur requirement is defined as ratio between blur and exit pupil diameter) is 0.59%, max pupil blur required is 1%, therefore compliance is verified.



BLUR	589 nm	800 nm	1650 nm
Nominal BLUR (radius, mm)	4.93	4.02	2.48
BLUR (radius, mm) 90% statistical coverage	6.33	5.34	3.62
Exit Pupil radius (mm)	1069.37	1069.37	1069.37
Ratio (% of pupil diam.)	0.59%	0.50%	0.34%
Ratio (% of pupil diam.), spec	< 1%		

Distortion

We considered the maximum value of distortion (at the pupil edge), directly computed as a percentage of the pupil radius. The exit pupil distortion is basically insensitive to the tolerances defined.

Table 15. Pupil quality tolerance analysis summary: pupil distortion. The computed max distortion is 0.031%, max pupil blur required is 1%, therefore compliance is verified.

DISTORTION	589 nm	800 nm	1650 nm
Nominal DISTORTION (%)	0.03%	0.03%	0.03%
DISTORTION (%) 90% statistical coverage	0.031%	0.031%	0.031%
DISTORTION (%), spec	< 1%		

Shift

The pupil shift is sensitive to SM tilt and W decenter (worst offenders). The analysis suggests halving the tolerances on SM and W tilts (0.005°) and decenters (0.1 mm). However, the CUFM DoFs will be very effective to precisely align the PUA exit pupil (will play a major role as compensators), so we expect to achieve much lower values of shift after the completion of the PUA-MORFEO alignment.

Table 16. Pupil quality tolerance analysis summary: pupil shift. The computed max shift (the shift requirement is defined as ratio between shift and exit pupil diameter) is 0.95%, max pupil shift required is 1%, therefore compliance is verified.

SHIFT	589 nm	800 nm	1650 nm
Nominal BLUR (radius, mm)	0	0	0
SHIFT (radius, mm) 90% statistical coverage	10.07	10.2	10.15
Exit Pupil radius (mm)	1069.37	1069.37	1069.37
Ratio (% of pupil diam.)	0.94%	0.95%	0.95%
Ratio (% of pupil diam.), spec	< 1%		



Position

The exit pupil position (distance from PUA output focal plane) is sensitive mostly to the W-SM distance. The defined set of tolerances introduce a variation of the exit pupil position of about 0.6% (standard deviation). Considering a variation of 1%, basically the entire statistic is covered.

5.4 F-number

The PUA internal pupil diameter is defined through a thin pupil mask, placed in front of the PM. Ideally, the pupil mask should be placed onto the pupil plane (PM optical surface), practically it will be placed as close as possible to it. The pupil mask diameter and its manufacturing tolerance are defined so that the PUA output f-number (NGS) matches the ELT f-number of 17.745 with the required accuracy of 1%. The analysis on the nominal optical design shows that with a pupil stop diameter of 105.2 mm the working f-number is 17.745 and that the accuracy of its reproduction (1%) is fulfilled with a tolerance of 0.4 mm. A much smaller tolerance will be defined on the pupil mask diameter and achieved with the pupil mask machining process, therefore output F-number compliance is verified.

5.5 Ghosts and stray light

As for the preliminary design, the main disadvantage of the new design is the presence of many beam-splitter surfaces, with a final very low throughput and the presence of ghosts and stray light. The presence and impact of ghosts and stray light has been evaluated during the PDR and will be minimized through a proper design of baffles and vanes during the Final Design phase. The final design of the baffling, as well as their implementation, and a complete ghost and stray light analysis (closely related to the baffling design), will be outsourced.

For the time being, we consider valid the results of the analyses carried out for the PDR (summarized below), since the most prominent ghosts originate at the surface of the CBS facing the PM, which is basically unchanged in the new PUA optical design (the distance PM-CBS is actually 2 mm larger, with more defocused ghosts as a consequence). The presence of the wedge on the BS1 and BS2 contributes to move away from the calibration optical path any ghost contributions from these components. The impact of the lenses added to the LGS optical path shall be evaluated during the preparation for the FDR. The same considerations can be applied to the stray light analysis, which is mostly unaffected by the new design layout since the foreseen AR coating are unchanged and the number of optical elements is unchanged in the NGS optical path and only slightly changed in the LGS optical path.

Finally, the possibility to push the performance of the CBS coatings through innovative processes (e.g. Random Anti-Reflection coatings) has been preliminarily explored and will be evaluated during the final design phase.



5.5.1 Ghost PDR analysis summary

Despite the large number of semi-reflective elements, the nominal (best-aligned) PUA design does not suffer from a severe ghosting problem on the output focal planes. All the channels have been studied with non-sequential Zemax designs to spot possible ghost features down to $10^{-7/8}$ relative irradiance factors. The heuristic approach based on geometrical considerations and the non-sequential ray tracing agree on the main results. No particular/peculiar ghosts have been found with respect to the expected features coming from the semi-reflecting components (CBS, SM, W, etc.). Two most prominent ghosts are visible at a ratio of $\sim 10^{-2}$ with respect to the real PSF both in the NGS and LGS arms. These ghosts are generated at the CBS surface and their amplitude can be modulated by the anti-reflection coating of the CBS. Whilst at the NGS-LO WFS pixel sampling scale the ghosts are resolved from the real PSF, at the NGS-REF and LGS WFSs they appear to be significantly blended to the PSF. The ghosts impact on the WFSs has been evaluated in terms of relative irradiance with respect to the real PSF and for their perturbation to the centroid of the image spot within the WFS SA. For all the WFSs the centroid shift induced by the ghosts never exceeds the 3% of the pixel size. The orientation of the centroid shift vector is driven by the ghosts' position and it can vary among the different fields points within the FoV. The ghosts are static and their position might change only upon (re-)alignment of the parent optics within the PUA. The transposition of these ghost-induced centroid shifts into WFS slope errors will be performed by the FDR. In an operative scenario we expect that the centroid within the SAs will be influenced also by the light sources apodization that is impractical to simulate and shall therefore be measured with the real optical fibers and the real LGS sources. An additional perturbation of the spot centroids will be posed by the optical geometric distortions within the PUA, MORFEO and the WFS optics. For these reasons we envision to map the centroid positions within the WF SAs for the system as-built and as-aligned in the Bologna Integration Hall (BIH). The measurement shall lead to a sort of look up table that accounts for the overall systematic contributions (ghost, apodization, distortion, tolerances) that shall be detrended from the slopes measured on sky.

The alignment and re-collimation procedure of MORFEO using the defocused PSF from the CU light sources is unaffected by the presence of the ghosts.

The average reflectivity at the interface between the glass, uncoated, optical surface and the air is about 4-5% for many commonly used materials. The use of an AR coating at R1%-R3% for the CBS decreases the ghost relative amplitude to about 0.14%-0.38% the real PSF

5.5.2 Stray light PDR analysis summary

The SL analysis of the PUA has been carried for three different scenarios: no scattering and two different scattering models. The PUA throughput computed considering a low level of dust (first scattering model) is: 0.15% for NGS, 0.5% for LGS.

Despite the low throughput, the estimated achievable SNR and the equivalent apparent magnitudes to the WFSs are suitable for the AIV operations and validation of both the CU and MORFEO and the WFSs calibration procedures also for the most severe scattering model.

The scenario suffering the lowest SNR is related to the validation of the CU pupil uniformity, being this plane uniformly illuminated and not an in-focus PSF. To collect a sufficient SNR



(>> 3) one option investigated is a pupil imager placed downstream the PUA output focal planes to re-image the pupil at a smaller scale, a few mm in diameter, to take advantage of the etendue factor and bypass the need for multiple mosaicking of the camera to patrol the full pupil. To overcome the issue of very low SNR for the LGS and REF sources PSF and pupils with the OWL1280 camera, a second camera with different detector size and no limitation of the maximum integration time might be required.

The alignability of MORFEO using the CU sources seems to be unaffected by the presence of ghosts and stray light.

The assessed low throughput of the PUA confirms the impossibility of using an interferometer in double pass for the alignment of the system end-2-end i.e. from the input to the output focal plane as well as for the final WFE verification. However, the interferometer can be used for the alignment of PUA subsystems, e.g. the “telescope” part (W+SM).

Preliminary simulations on the effects of the PUA mechanical structure (without the optics mounts) have not highlighted significant stray light contributions, also thanks to the presence of a preliminary set of baffles that block the most prominent stray light components.

5.5.3 Additional ghost analyses for OFDR

Additional analyses have been recently performed on the new design, to evaluate the impact of the “pupil ghost” found during the test campaign on the Paraxial Calibration Unit Prototype (PCUP, that faithfully reproduces the PUA NGS on-axis optical path).

The pupil ghosts are created by the optical rays that travel through the “telescope assembly” (SM+W) only once (Figure 26), since W lower surface has a 50% beam-splitter coating. These rays reach the PUA output focal plane only mildly converging and propagate to the nominal pupil plane, resulting in a bright spot potentially overlapped to the pupil image. In general, each PUA source generates its ghost, but the overlap between ghost and pupil image is limited to the on-axis source, as shown in Figure 27: the sources placed at the minimum off-axis distance (16 mm = 18”) fall out from the exit pupil image, and the more the source is off-axis, the more is the ghost distance from the pupil plane (linearity).

It is worth noting that, unfortunately, the ghost produced by the PUA on-axis source cannot be removed from the system in the nominal design: it cannot be disentangled (by tilting W) due to unacceptable WFE induced on LGSs and there is no possibility to dump it down to an acceptable level (re-optimizing the PUA optical design). However, the analysis shows that the pupil ghost size and position on the REF-WFS pupil plane are not a problem for the calibrations, as well as its level of intensity on the WFS detector.

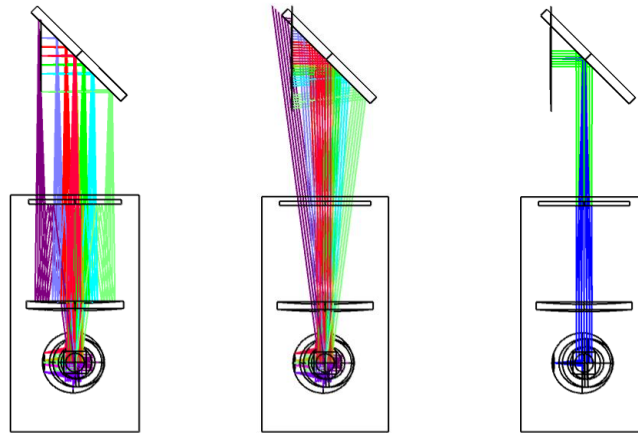


Figure 26. PUA sources ray-tracing: nominal paths (left), ghost paths (center), on-axis source nominal -blue- and ghost -green- paths (right).

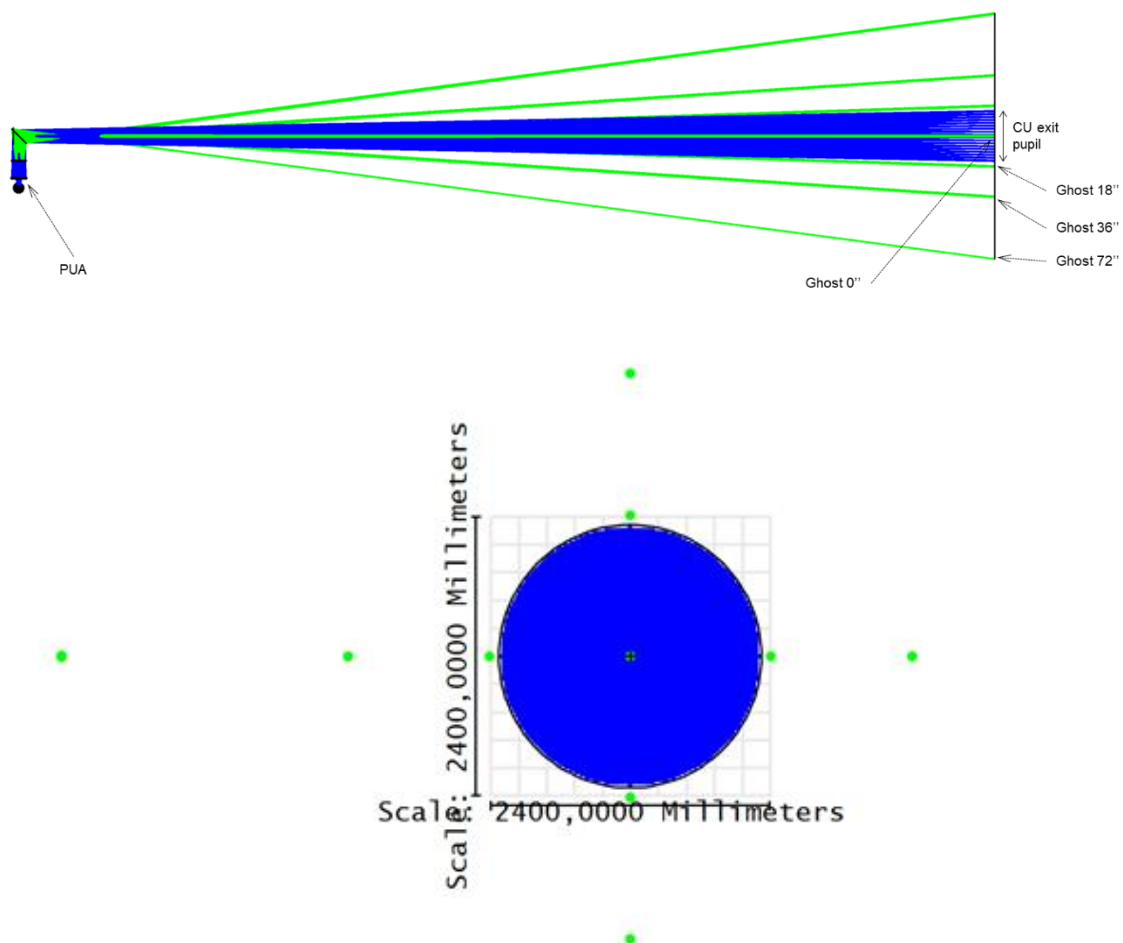


Figure 27. (top) PUA sources ray-tracing up to the exit pupil plane: nominal path (blue), ghosts' paths (green). (bottom) PUA sources footprints on the pupil plane: nominal paths (blue), ghost paths (green). With the exception of the on-axis source ghost, no ghost falls on the pupil image.



By including MORFEO and the REF-WFS to the optical model, it is possible to extend the ray-tracing down to the lenslet and detector level, to check size and source of the on-axis source ghost (Figure 28). The on-axis source ghost falls within the central 4 subapertures of the REF-WFS (lenslet array: 8x8 subaps, 30x30 pix/subap -> 240x240 pix, 24 $\mu\text{m}/\text{pix}$). A geometric image analysis is performed to retrieve PSFs and ghost relative intensity (Figure 29). The source is considered uniform, 400 μm in diameter (REF Multi-mode fiber), the detector's size is 5.76 mm (with 240x240 pixels). The PSF peak irradiance is 5.9 W/mm^2 . The ghost rms irradiance is 0.0126 W/mm^2 . Considering a “telescope” transmission factor (nominal/ghost) of 0.25, the final ratio between PSF peak intensity and rms ghost intensity on the REF-WFS detector is 117.

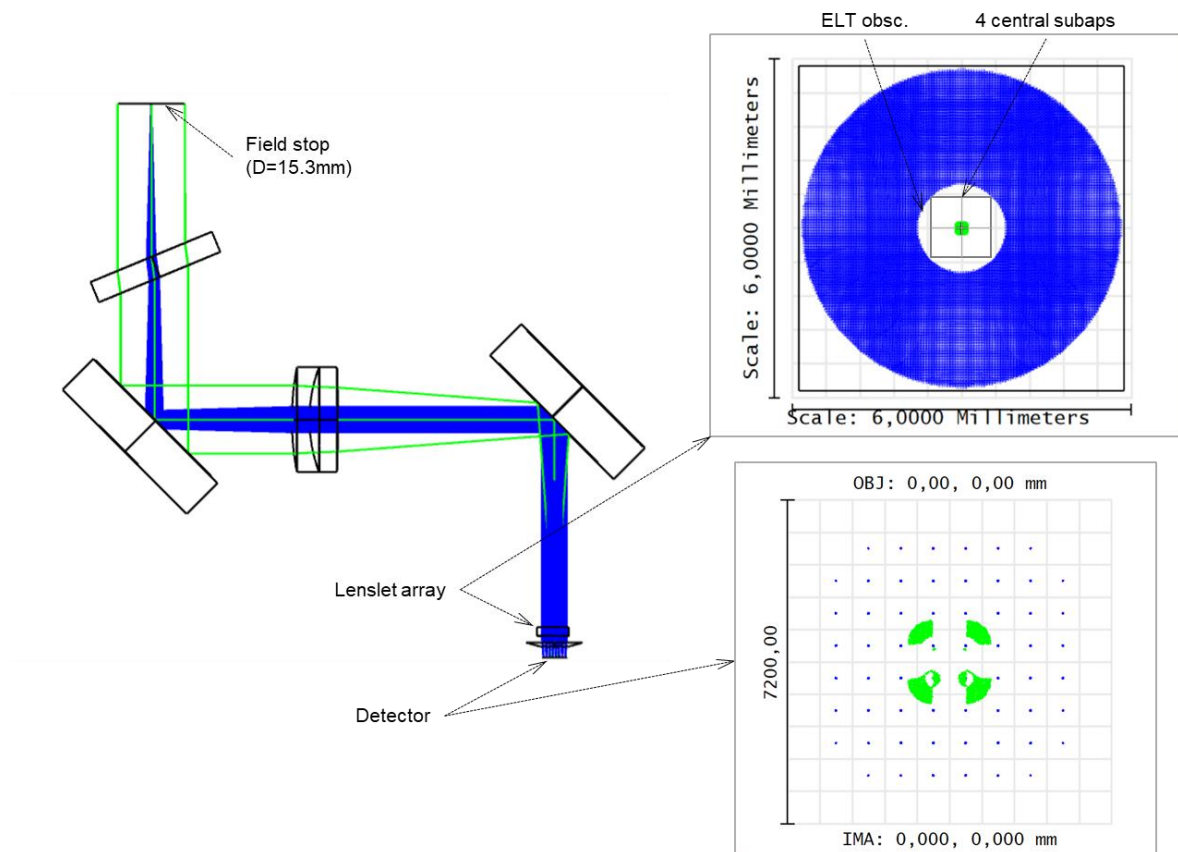


Figure 28. Ray-tracing of the PUA on-axis source (nominal path in blue, ghost path in green) down to the REF-WFS: footprints on the conjugated pupil plane (lenslet) and spot diagram on the detector focal plane. REF lenslet array: 8x8 subaps, 30x30 pix/subap -> 240x240 pix, 24 $\mu\text{m}/\text{pix}$.

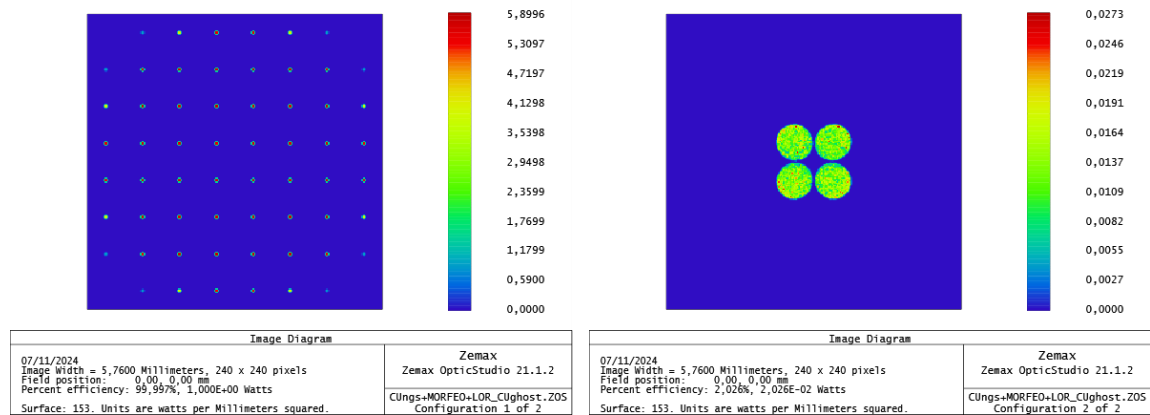


Figure 29. REF-WFS detector's image analysis: nominal PSFs (left), ghost (right).

5.6 Optical alignment

See AD2.



6. Mechanical design review

6.1 Preliminary mechanical design review

The PUA preliminary mechanical design revision process highlighted two main criticalities:

- Difficulties in fulfilling the assigned mass budget requirement.
- Limited access to key areas of the volume, with resulting difficulties in the machining and in the alignment process.

The new optical design has driven the mechanical re-design, which has been only addressed in a preliminary way and which will be outsourced.

6.2 The new mechanical concept

6.2.1 Structure

The PUA main tubular frame has been retained, slightly modified to satisfy the new needs and solve the previous construction difficulties. The new mechanical design foresees a single welded structure (main frame, Figure 30 left) that supports the “telescope” assembly (Figure 32), equipped with sub-structures (highlighted in different colors in Figure 30 right) to support the remaining optics and mechanical sub-assemblies with easily workable support interfaces.

The manufacturing processes of all the mechanical and opto-mechanical structures will be defined by the Contractor, to ensure their precision and stability over time.

According to the new mechanical concept:

- The pink (#1) and green (#2) supporting structures (Figure 30 right) will be machined to guarantee precise interfaces, as well as the interface plates of BS2 and EM sub-assemblies, directly fixed on the main frame (Figure 31).



Figure 30. PUA mechanical concept: main frame on the left (the yellow beam shall be dismountable) and supporting structures on the right (highlighted in pink and green, respectively).



- The LGS supporting structure (highlighted in green in Figure 30 and Figure 31) will be machined and assembled outside the main frame, then easily fixed to it, with the optical elements fully accessible from the outside.
- The structure supporting PM, CBS and BS1 (highlighted in pink in Figure 30 and Figure 31) will also be machined and assembled outside the main frame, then easily fixed onto it. A mechanical interface is foreseen on this supporting structure, to mount the pupil sources in correspondence of the pupil plane positioned below the CBS.

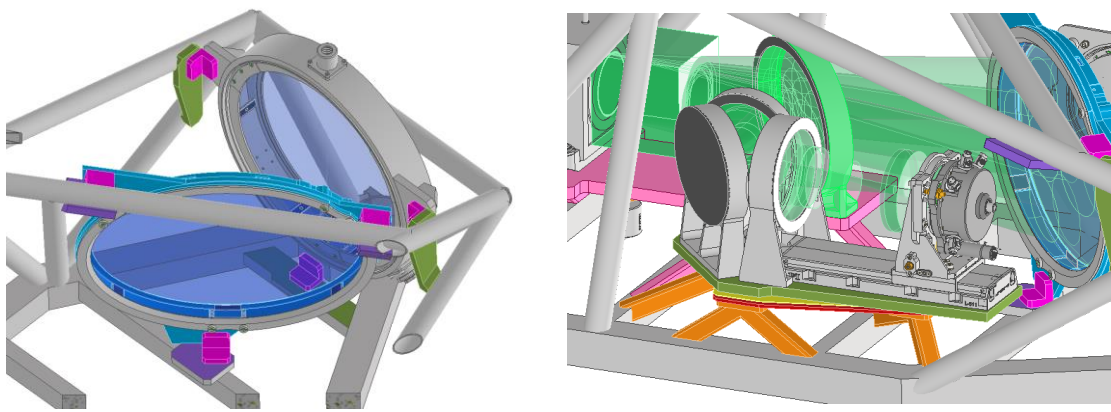


Figure 31. PUA mechanical concept: BS2 and EM directly fixed on the main frame (left), LGS bench (right).

- The “telescope” (TEL) frame, supporting both W and the SM, will be assembled and machined, and the opto-mechanics fixed on it and mutually aligned (Figure 32). The TEL assembly will finally be fixed onto the main frame and aligned to the rest of the optics.



Figure 32. PUA mechanical concept: “telescope” assembly.



A conceptual design including baffles and vanes against stray light and an external cover has also been developed (Figure 33).

The integration of the PUA into MORFEO will be performed through 4 Ball transfer units (Figure 33). Procedure and equipment will be detailed during the final design phase.

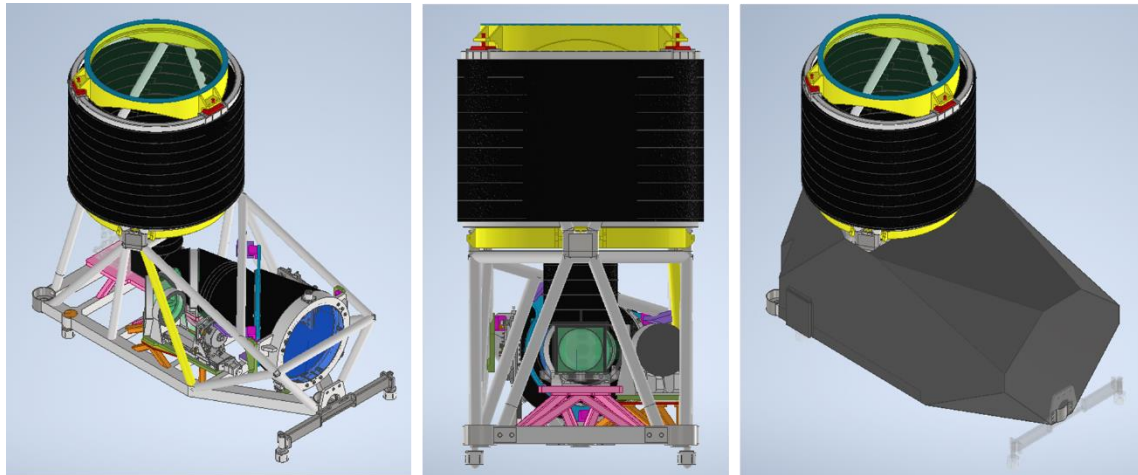


Figure 33. PUA mechanical concept: baffles are highlighted in black, external cover in grey (right).

6.2.2 NGS mask assembly (NGSM)

The NGS mask assembly (NGSM), shown in Figure 34, hosts all the fibers that inject the NGS sources into the PUA optical relay, ensuring a proper illumination of the PUA internal pupil.

It is composed of:

- mask plate, holding all the fiber connectors;
- flanges, for the connection to the mechanical structure and the adjustments;
- adjustment system, for the proper alignment of the mask plate.

Although size and shape of the mask are essentially driven by the optical design, its manufacturability has been taken into account during the optical design optimization. The main design drivers for the assembly have been: the mask plate geometry (size and shape), the source pattern geometry (number, displacement and separation), the sources size. Moreover, since the fibers are attached to the mask through connectors, every connector adapter seat needs a precise machining, so that each fiber has the correct focal position and chief-ray direction. The mask layout and design are shown in Figure 34 and Figure 35. The mask is ~170 mm in diameter, with a RoC of 372.57 mm, and hosts a grid of 7 by 7 sources, regularly distributed across the technical FoV (160"), surrounded by 12 more external additional sources, for a total of 61 NGS sources. Among them, 25 are REF+LO coupled sources (by means of dual-core ferrule, see Figure 36). The 9 central sources (the NGS-MIC sources placed within the MICADO FoV), are single sources, with the exception of the central one (the on-axis source), coupled with a REF source.



Special fiber terminations are needed to produce the REF+LO/MIC double-sources (also called “coupled-sources”), since it is required to couple sources of different size (and hence different cores size) as schematically represented in Figure 36. A 400um core multi-mode fiber is used for each REF source and a 9 um core single-mode fiber for each LO/MIC source. Each fiber pair will be terminated in a custom dual-core ferrule, providing an inter-axial distance of ~440 um.

The large number of connectors (61) to place onto the convex mask has required a careful evaluation of the physical separation among connectors and thus of the space available for their mounting and dismounting. The available space is not sufficient to replace them with bare hands, and a special tool has been conceived to easily connect and disconnect the fiber terminations (Figure 34). The goal of accommodating 121 sources cannot be met due to opto-mechanical constraints. Placing such a high number of fibers and connectors on a mask with a diameter of 170 mm would reduce the distance between adjacent fiber axes to 9.5 mm, compared to the current distance of 16 mm. This reduction is unfeasible for two main reasons: the selected connectors have a diameter of 10.8 mm, and this setup would prevent access to individual fibers, even with specialized tools. Alternative solutions would involve outsourcing the NGS mask with glued (non-replaceable) fibers, leading to difficult and potentially hazardous handling during the MAIT and AIV phases. Ultimately, the current configuration represents the best trade-off among total number of fibers, fiber splitting solutions, accessibility, simplicity and cost.

The mask RoC directly controls the output focal plane RoC, so in case the ELT as-built focal plane RoC is different from the nominal one (the last used to optimize the mask RoC), it will be sufficient to slightly re-optimize just the mask shape to recover the optimal performance. The flanges are necessary to connect the NGSM to the PUA mechanical structure and to allow its adjustments. The NGSM is provided with an adjustment system for decentering, focus and tip/tilt. Four screws (the grey ones in Figure 34) allow to correctly align the mask with the optical axis, while three further screws (the orange ones in Figure 34) set the focus and the tip/tilt of the mask. The range for the focus adjustment is ± 3.7 mm, the range for the tip/tilt adjustment is ± 1 deg, the range for the decentering adjustment is: ± 5 mm.

A (blackened) baffle-mask is positioned in front of the fiber tips (see Figure 35 right) and defines the beams' f-number coming out from the mask. Their holes are sized so that the output cones are slightly larger than the nominal ones (output NGS beam f-number is 4, nominal NGS beam f-number is 4.7), with the remaining light in excess stopped by the pupil mask.

The fiber terminations (FC/PC connectors) are multiplied by means of custom single-mode (SM) and multi-mode (MM) fiber splitters for the LO and REF sources respectively. For each single source a termination is used, while custom dual core ferrules are used to provide the coupled LO and REF within the LOR WFSs FoV.

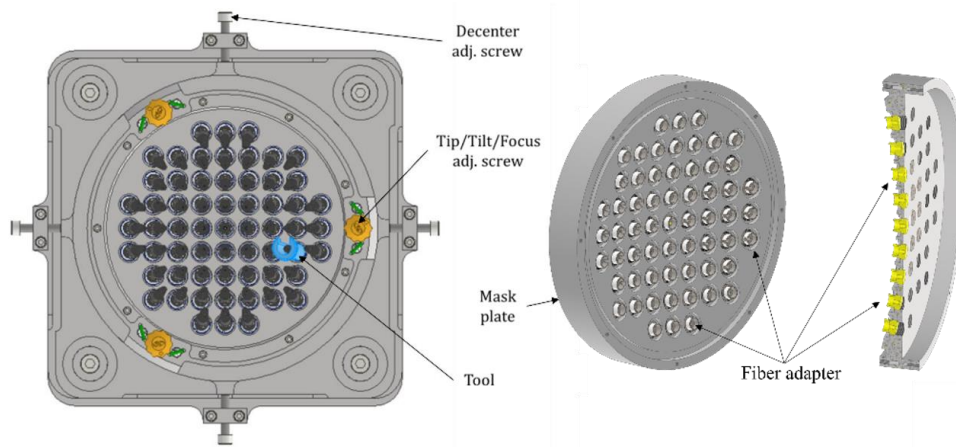


Figure 34. 3D model of the NGS mask and its adjustment system. A dedicated tool is used to mount and dismount the FC/PC connectors from the mask. On the right, a section view of the mask showing the arrangement of the fibers to obtain the correct focal position of each fiber tip, and the optimal alignment of each fiber axis in terms of chief-ray angle.

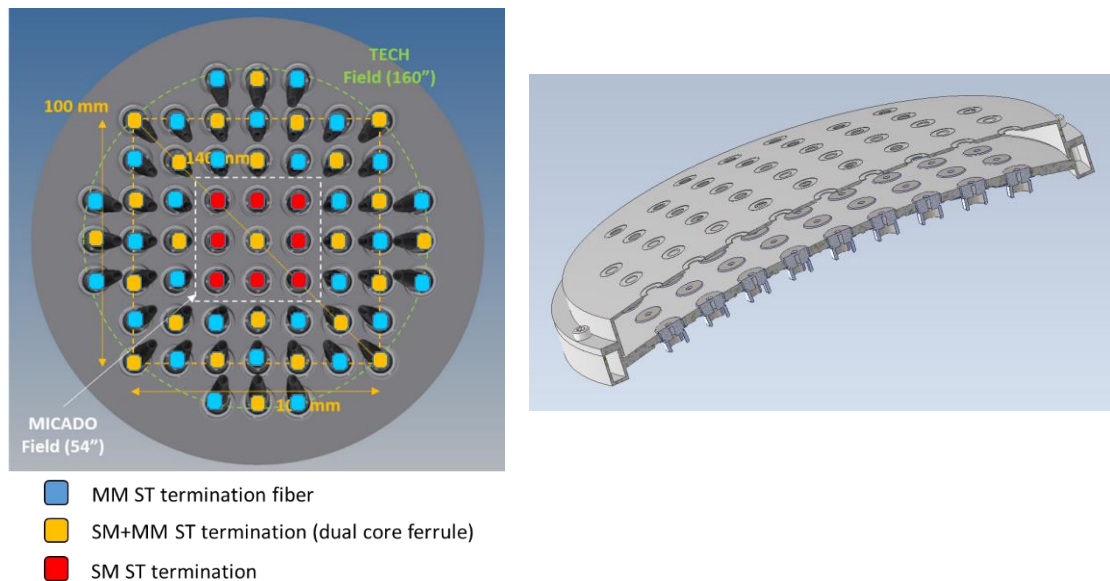


Figure 35. *(left)* NGSM sources layout. The cyan-marked sources are REF(-only) sources, evenly distributed across the field. The 8 central sources marked in red are MIC sources, used for MICADO (DL @ 1650 nm, angular diameter of ~10 mas on-sky). All the 25 sources used for LO are coupled with REF sources in close doublets and are marked in orange. They are as much as possible evenly distributed across the field, each couple is composed of a REF source (800 nm of central wavelength, angular diameter ~450 mas on-sky) and a LO source (having the same characteristics of the MIC source). The on-axis source is also a LO/REF double source. *(right)* NGS mask cut view, with the front holes acting as baffles and defining the NGS mask output f-number.

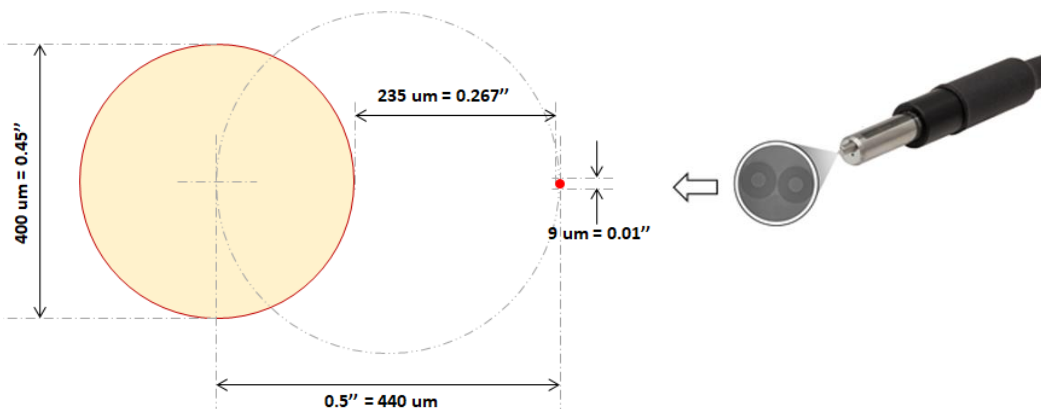


Figure 36. Geometry of the dual-core ferrule needed to realize the REF+LO/MIC double source. The core diameter is 9 μm for the LO and 400 μm for the REF, the distance between the two core centers is $\sim 440 \mu\text{m}$.

Laboratory tests using several SM and MM fiber types (Figure 37) on a representative laboratory testbed, have allowed to check the intermediate pupil uniformity to verify to stay within the 20% of flux variation across the fully illuminated sub-apertures of the NGS WFSs. As expected, the Gaussian profile of single-mode fibers can hardly guarantee the compliance with the requirement, due to the significant intensity variation between the center and the edges of the pupil. However, to overcome this issue, unconventional fibers from Thorlabs, called Ultra-High Numerical Aperture (UHNA), have been tested. They have higher numerical apertures than standard silica fibers, with lower bend loss, and operate at wavelength ranges similar to those of the SMF-28 Ultra fiber. The selected fiber is the UHNA7, operating above 1500 nm (second mode cut-off at 1450 nm), with a numerical aperture (NA) of 0.41 and a mode field diameter (MFD) of 3.2 μm at 1550 nm.

As a result of the laboratory test, the UHNA7 fiber illuminates the pupil with a more uniform intensity distribution, presenting a shape similar to a super-Gaussian profile. Some edge effects have been measured at the pupil plane and, although negligible, they will be further investigated. Moreover, the smaller core ensures the achievement of a higher Strehl Ratio (SR): for the LO/MIC sources, with a $\text{MFD}@1650\text{nm} < 5\mu\text{m}$, it is expected a $\text{SR} > 85\%$. Therefore, the use of this type of fiber significantly improves the performance of the Calibration Unit in emulating DL sources. Conversely, because of the larger NA, the single-mode beam coming out from the mask will be much larger than that required ($\text{NA} \sim 0.11$), thus resulting in a large loss of the input flux. Although we foresee a limited impact on the LO/MIC overall throughput (see the very high P_{ratio} computed for these sources and reported in Table 23), this loss and its effect will be carefully considered and estimated.

Multimode fibers are used to emulate extended sources (REF) with a very broad wavelength range. They are fed by halogen lamps that provide a broad band spectrum from 0.6 to 1.0 μm . The pupil intensity plots show a flat-top shaped profile for both the tested fibers, therefore, if no other significant differences will be found, the final choice will be driven by the NA, which shall not be much larger than the NGS nominal output beam NA (~ 0.11).

A further issue that typically affects MM fibers is the presence of cladding modes. While most light in a MM fiber is guided by total internal reflection within the core, higher-order modes could propagate in the cladding layer. They cause a signal loss due to bending and can modify the beam spatial profile. The prototyping of the mask and further tests on MM fibers will allow a better evaluation of these effects and, if needed, the identification of possible methods to remove them (e.g. mandrel wrapping or modes scrambling).

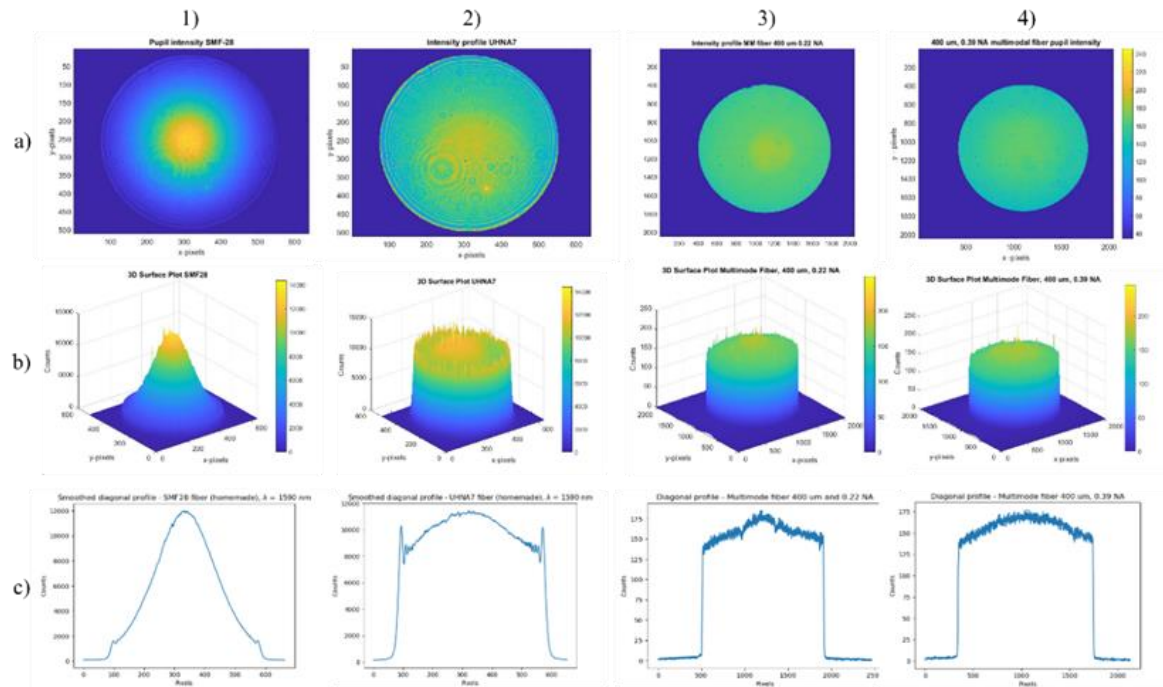


Figure 37. Comparison of SM and MM fibers used for the laboratory tests: a) 2D pupil uniformity; b) 3D pupil intensity distribution; c) 2D pupil intensity profile. Each column shows the results for a tested fiber type: 1) Thorlabs SMF-28 Ultra; 2) Thorlabs UHNA7; 3) Thorlabs FT400EMT; 4) Thorlabs FG400LEA.

6.2.3 LGS mask assembly (LGSM)

Unlike NGS sources, LGS sources are generated through a pinhole mask, backlit by a *Lightbox* that has the same function of an integrating sphere. This choice was necessary to provide sources with a diameter of 2.9 mm and 3.3 mm on the mask (3" on sky), ensuring a proper illumination of the PUA pupil. The focal position depends on the LGS conjugation height (as well as the LGS asterism to be used): a linear stage with a minimum travel range of 170 mm is necessary to place the assembly to the proper focal position.

The LGS Mask Assembly (LGSM, Figure 38 and Figure 39) is composed of:

- A mount, attached to the linear stage;
- The lightbox, mixing the light coming from more fibers;
- The pinholes mask, defining the sources size and position;
- A black cover (light absorbing material);
- A motorized shutter, to stop the light coming out from the unselected asterism;
- A fixed secondary diaphragm (baffle-mask) to prevent stray light diffusion, through holes sized so that the output cones are slightly larger than the nominal ones (output LGS beam f-numbers are 4.3 and 5.0, nominal LGS beam f-numbers are 5.15 and 5.9), with the remaining light in excess stopped by the pupil mask;
- An adjustment system for the alignment of the whole assembly.

To backlight the mask, four MM fibers, each fed by a narrow-band (central peak at 590 nm) laser diode placed in the CU Electronic Cabinet, inject the light into the lightbox, internally



coated with a high diffuse reflectance material (e.g. *Spectralon*). Since the incident light is completely diffused after internal multiple reflections, the lightbox will provide output beams with a uniform flat-top profile at the pupil plane. Such a solution is also advantageous from the point of view of the LGSM availability, since the redundancy of the fibers (each one fed by a laser diode) allows to keep the system in operation in case of failure of a physical source.

The mask is a backlit flat pinhole mask, ~110 mm in diameter, with two regular asterisms of six sources each ($\Phi 2.9$ mm for LGS-104km, $\Phi 3.3$ mm for LGS-150km), as shown in Figure 39. The two asterisms are mutually rotated of ~23 deg, to simulate the mutual rotation of the two LGS asterisms (@104 and @150 km) on sky. A rotating shutter has been implemented to select only one asterism of LGSs at a time, therefore preventing the stray light that would come from the other (out-of-focus) asterism. The three orange screws mounted on the pinhole mask provide tip/tilt adjustment capabilities (± 2 deg), while the mask decentering is adjusted thanks to two screws on the mount.

A central source (and related pinhole) has been added to the mask for alignment purposes during the system AIV. It has no specific quality requirement and is provided by means of an optical fiber connected to the rear of the lightbox. It can be fed by one of the spare fiber terminations already present in the PUA (thus allowing to inject both a visible and/or infrared beam).

Since the lightbox design significantly differs from a standard integrating sphere (cylinder vs sphere), it will be important to prototype the assembly and test it, to verify its intrinsic efficiency with respect to that of an equivalent (same internal area of reflection) standard integrating sphere. In this way, the final throughput will be better estimated.

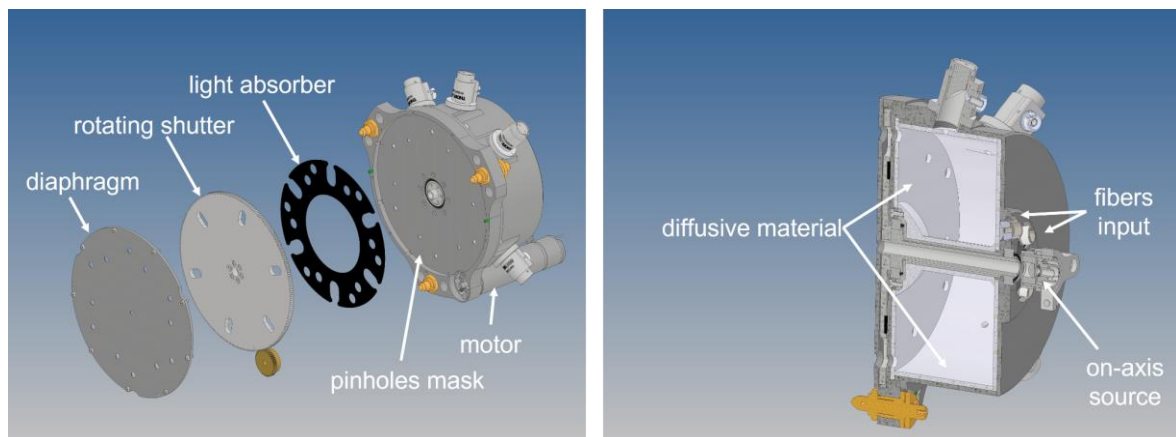


Figure 38. 3D model of the LGS mask assembly (LGSM): on the left, an exploded view of the front components; on the right, a section view of the lightbox, showing the internal high reflectance diffusive covering, the fiber inputs and the central source used for alignment.

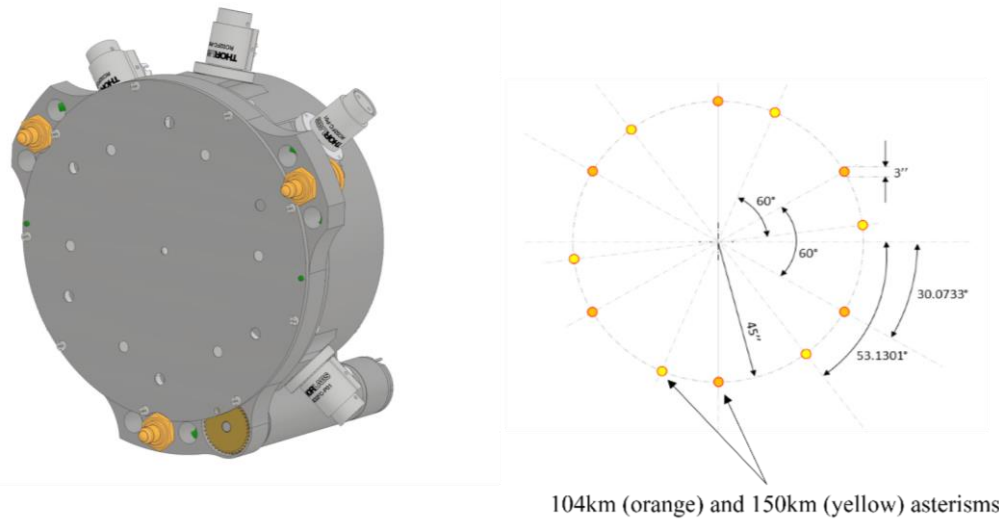


Figure 39. (left) 3D model of the LGSM (front view), (right) Geometry of the two asterisms conjugated at 104 km (orange) and 150 km (yellow).

6.2.4 Pupil Sources Assembly (PSA)

The Calibration Unit will also provide some additional sources, called “Pupil Sources” (PS), placed on the internal pupil plane. Since the nominal pupil plane is occupied by the PM, these sources will be placed underneath the CBS, where a second pupil plane is available. The pupil sources are required to support the PUA mutual alignment to MORFEO and to the SCAO WFS and to support the verification of the MORFEO exit pupil requirements. To perform these tasks, a suitable light panel will be used, with a pinhole mask placed on its diffusing surface. The PS panel will be probably fed with an optical fiber (or fiber bundle) to avoid heat deposition within the PUA, and will be mounted on an adjustable (piston, tip, tilt) support, for its integration and proper positioning. A detailed description of the PSA will be provided for the FDR.

6.3 Structural aspects

The main supporting structure (composed of main frame and “telescope” frame) has been optimized in the tube sections thanks to a flexible finite element model (Figure 40) – modeled through “beam” elements – where the non-structural elements have been replaced by their equivalent masses.

The FE Analyses (FEA) performed to check the adequacy of the new PUA mechanical design, as well as the verification criteria, are summarized in Table 17. The results of the analyses are shown in Table 18 and Figure 41.

Table 17. Analyses and verification criteria applied to the simulations.



Analysis	Verification	Requirement / Criterion
Modal	Eigen-frequencies	First Eigen-frequency (f_1) > 30 Hz
Earthquake	Resistance to stresses induced by earthquake	Safety Factor (SF) > 1.5
Buckling	Buckling conditions	Safety Factor (abs. value) > 10

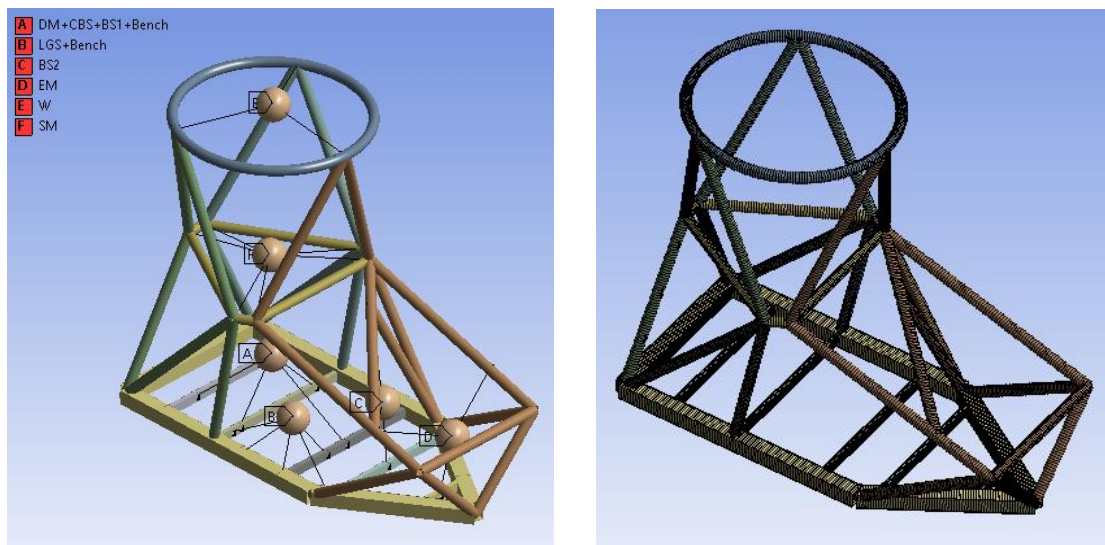


Figure 40. PUA finite element modeling: “beam” model with the main loads (left), meshed model (right). Simulations performed with the software *Ansys*®. Masses applied to the model (kg - entity and distribution deriving from assumptions partly based on the preliminary design): A=50, B=35, C=20, D=25, E=30, F=70, Tubes=60.

Table 18. Results of Modal Analysis and Buckling Analysis by FEAs. The Safety Factor (SF) for buckling analysis corresponds to the Load Multiplier value. Compliance is verified.

Modal		Buckling	
Mode	Frequency [Hz]	Mode	Load Multiplier
1,	66,81	1,	-245,81
2,	78,165	2,	-244,93
3,	95,603	3,	-206,48
4,	117,24	4,	-206,12
5,	129,16	5,	-132,82
6,	138,76	6,	-132,73
7,	162,49	7,	-108,28
8,	177,62	8,	-108,27
9,	192,47	9,	278,13
10,	223,37	10,	278,31
$f_1 = 67$ Hz Min f_1 required = 21 Hz		SF min = 108 Min SF required = 10	

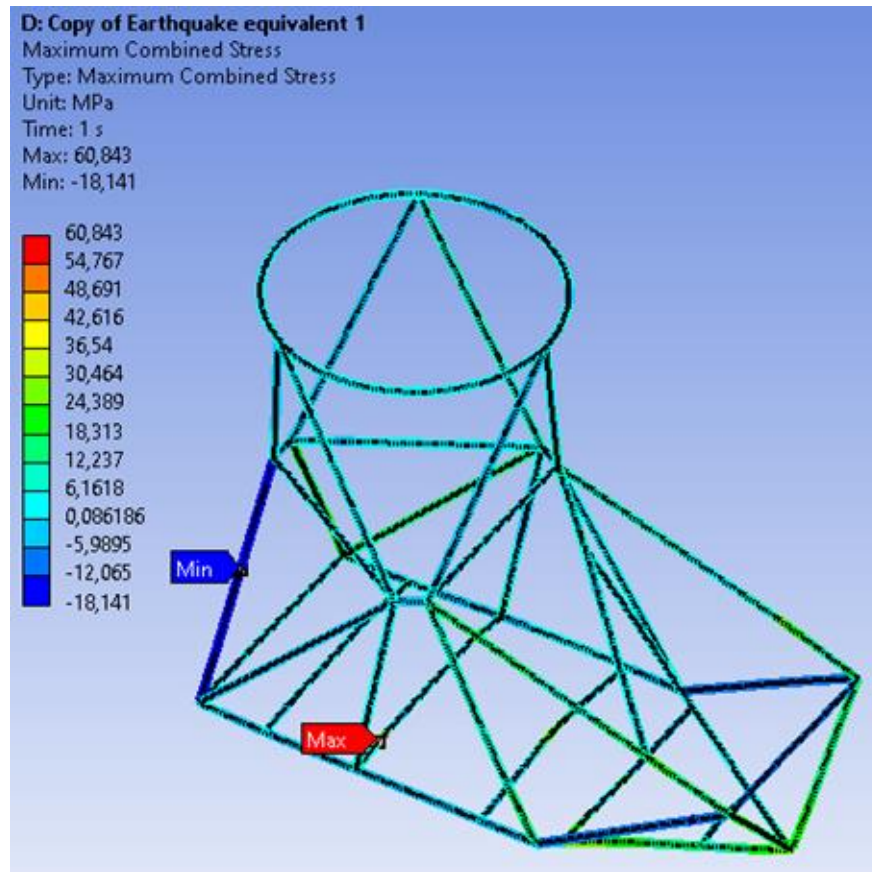


Figure 41. Results of the Earthquake Analysis by FEAs (worst combination of $a_x=\pm 3.3g$, $a_y=\pm 3.3g$, $a_z=\pm 2.185g$). The Safety Factor (SF) is computed assuming the structural steel S235, as the ratio between the admissible stress (yield limit reduced by 30% in correspondence of a seam) and the maximum stress in the worst combination of equivalent earthquake accelerations: $\sigma_{eq,max} = 61 \text{ MPa}$
→ SF = 2.7. The minimum SF required is 1.5 therefore compliance is verified.

6.4 Opto-mechanical aspects

In the new optical design, the thickness of W and SM has been reduced, and therefore the gravitational deformation and the associated optical aberrations will be higher. The opto-mechanics of these two components have to be carefully designed, in order to minimize the amount of non-axisymmetric deformations. The definition of type, amount, and disposition of the support points of the optics is propaedeutic to the design of their opto-mechanics, whose complexity increases with the number of support points, while the optical deformation decreases.

A trade-off analysis has been carried out of both W and SM to establish the best configuration. Three support configurations of increasing complexity have been analyzed, first through FEAs to derive the gravitational deformation of the optical surfaces, then imported into the optical model to compute the WFE associated with those deformations:



- A) 6 isostatic axial support pads (3 bipods)
- B) 6 isostatic axial support pads (3 bipods) + 3 adjustable spring supports ($\pm 10\%$ of pre-load asymmetry)
- C) 6 isostatic axial support pads (3 bipods) + 6 adjustable spring supports (3 bipods, $\pm 10\%$ of pre-load asymmetry).

The results of the FEAs carried out on W are shown in Table 19, where histograms with the aberrations associated with the different deformations are also reported. It is evident how the spherical aberration component (Z11) does not depend on the mounting configuration, but only on the optical aspect ratio and the supports radial position. The astigmatism (Z5, Z6) present in the configurations with spring-loaded pads is the result of the asymmetry defined in the pre-load ($\pm 10\%$). Configuration A is the only one where a significant component of hexafoil (Z28) is present.

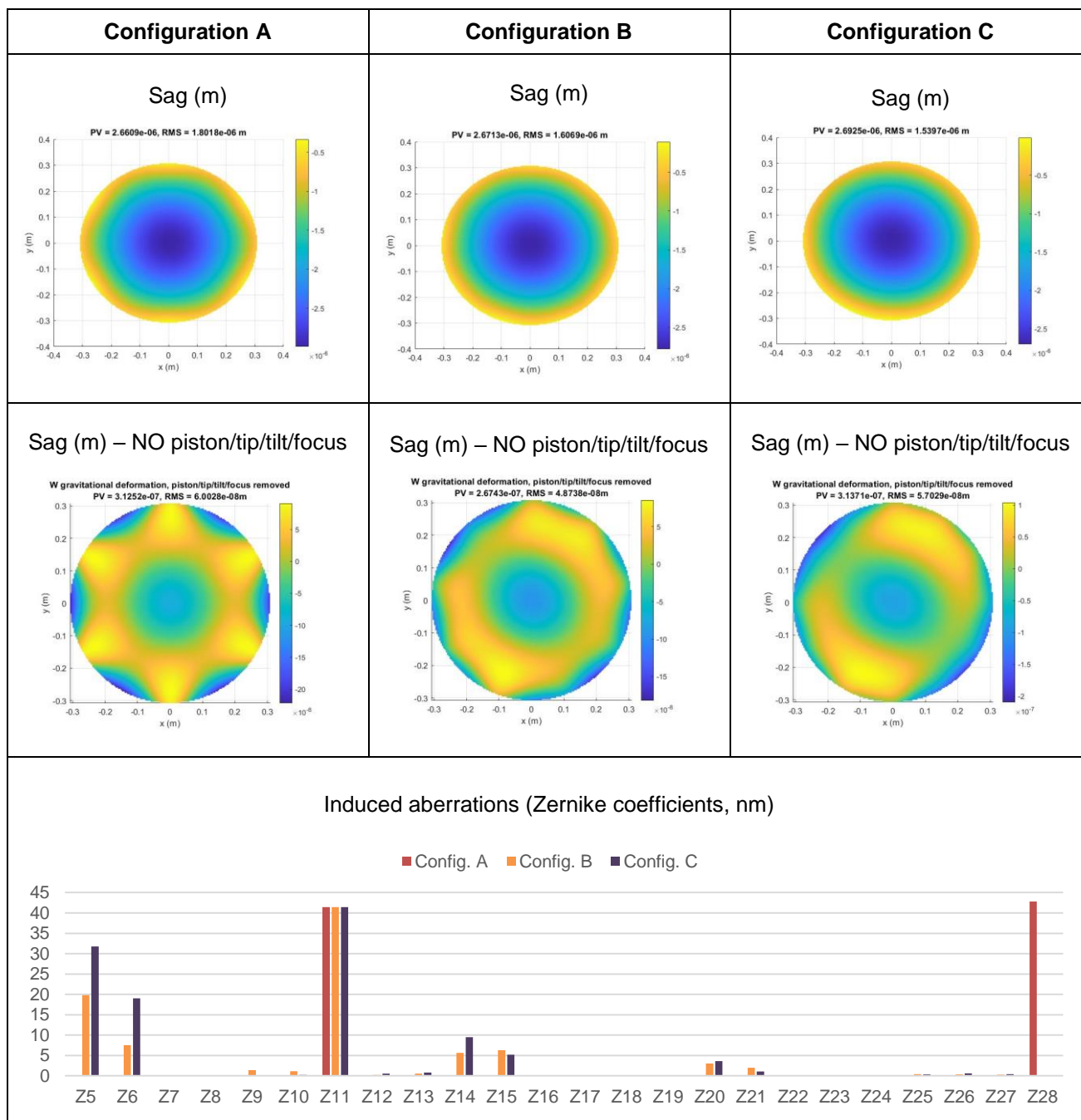
The deformations of SM are not reported as they are qualitatively identical to those of W, simply scaled because SM is stiffer (similar diameter but larger thickness).

The impact of these induced aberrations has been analyzed for all the possible combinations of supports and for all the different optical channels of the PUA. The most sensitive channel, as already known, turns out to be LGS-104km and the complete results (all possible combinations of support configurations) of induced WFE are shown only for this channel (Figure 42). The WFE introduced by the chosen combination is negligible for all the other channels. The plot of Figure 42 clearly shows that configuration C does not perform better than configuration B and that configuration A is not adequate for SM.

The best combination is configuration B for both W and SM.



Table 19. Results of FEA carried out on W (640 mm of mechanical aperture, 30 mm of thickness): gravitational deformation (sag) and associated aberrations (Zernike coefficients, *Noll* notation) for each configuration.



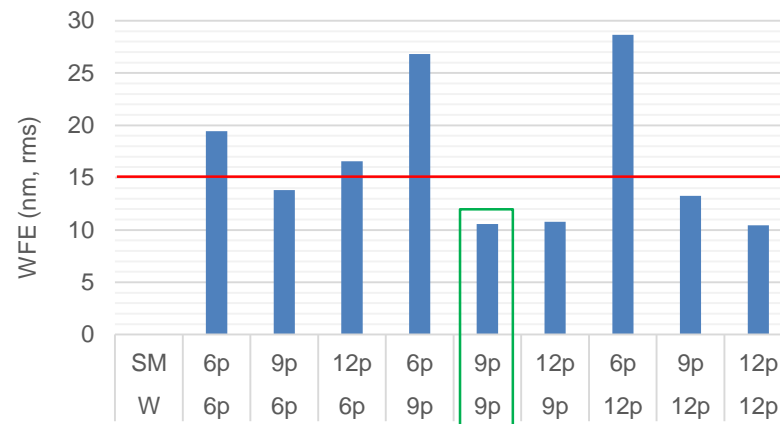


Figure 42. WFE (nm, rms) induced by W and SM gravitational deformation for the different support combinations. Naming: 6p = Config. A, 9p = Config. B, 12p = Config. C. A threshold of 15 nm has been considered and the best configuration is highlighted in green.



7. Throughput analysis

The whole CU transmission chain, sketched in Figure 43, has been analysed to evaluate the overall optical throughput for the NGS and LGS paths, to identify the main loss factors and possible criticalities. Once detailed and computed the overall transmission, from the physical light source (“Lamp”) to the output focal plane, the maximum required fluxes have been considered to verify the compliance of the selected physical sources in terms of power.

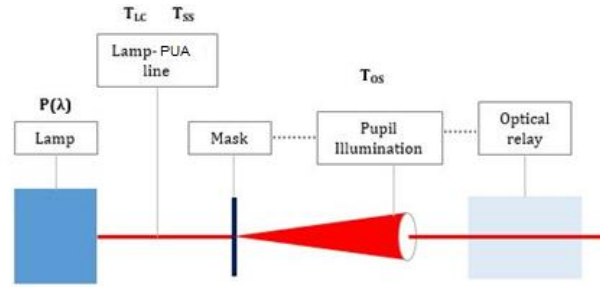


Figure 43. Scheme of the Calibration Unit transmission chain.

7.1 NGS path

Referring to the notation of Figure 43, the number of photons per second through the pupil (N_{ph}), over a spectral band $[\lambda_1, \lambda_2]$ can be computed as follows:

$$N_{ph} = \frac{1}{h c} \int_{\lambda_1}^{\lambda_2} T(\lambda) P(\lambda) \lambda d\lambda$$

where

h is the Planck constant

c is the Light speed

$P(\lambda)$ is the spectral power emitted by the physical source (“Lamp”)

$T(\lambda)$ identifies the total transmission (throughput) of the system, computed as follows:

$$T(\lambda) = T_{LC}(\lambda) T_{SS}(\lambda) T_{OS}(\lambda) F(\lambda)$$

$T_{LC}(\lambda)$ is the Lamp-PUA line transmission, computed as follows:

$$T_{LC}(\lambda) = T_{FL}(\lambda) T_{FC}$$

where:

$T_{FL}(\lambda)$ is the attenuation due to the fiber length (~40 m with a loss of 0.01 dB/m)

T_{FC} is the attenuation due to fiber discontinuities (4 discontinuities for the REF channel and 3 for the LO/MIC channels, with a loss of 0.3 dB each)

$T_{SS}(\lambda)$ is the transmission related to the fiber splitting system (2 splitters 1x8 for the REF channel and 1 splitter 1x16 for the LO/MIC channels). Reference values for the losses of the fiber splitters are provided by the manufacturers (see Figure 40).



Splitter type	1×2	1×4	1×8	1×16	1×32
Max. insertion loss [dB]*	4	8	11	15	18,5

Splitter type	1×2	1×4	1×8	1×16	1×32
Max. insertion loss [dB]*	3.9	7.0	10.2	13.5	16.7

Figure 44. Fiber splitters insertion loss for MM (top) and SM (bottom) applications. “Insertion loss” is the ratio of the optical power launched at the given input port of the splitter to the optical power from any single output port.

$T_{OS}(\lambda)$ is the optical system transmission (optical throughput) for the NGS path. The value, reported in Section 5.5.2, is multiplied by a factor 2 since in the new optical design BS1 has no longer a 50% beam-splitter coating but a dichroic coating.

$F(\lambda)$ is the geometrical dilution factor related to the pupil illumination, considering the cone angle coming out from the fibers and the cone angle associated to the NGS optical system f-number (Table 20).

Table 20. Dilution factor related to the pupil illumination (NGS channels).

Channel	Fiber $f_{\#}$	System $f_{\#}$	F
NGS-REF	2.27	4.7	0.24
NGS-LO/MIC	1.22	4.7	0.075

7.2 LGS path

The same approach described in the previous section has been followed. If not specified, the same assumptions and parameters have been applied.

$T_{LC}(\lambda)$ is computed considering 3 fiber discontinuities.

$T_{SS}(\lambda)$ represents the transmission at the level of the LightBox.

Considering this device as an Integrating Sphere, its transmission efficiency can be estimated as follows:

$$T_{SS}(\lambda) = \frac{\rho}{1 - \rho} \frac{A^{out}}{A_{sph}}$$

where

ρ is the internal reflectivity (0.98 for “Spectralon”)

A^{out} is the total output surface (sum of the pinholes areas – each pinhole has a diameter of ~3 mm)

A_{sph} is the LightBox internal surface



$T_{OS}(\lambda)$ is the optical system transmission (optical throughput) for the LGS path. The value, reported in Section 5.5.2, is multiplied by a factor 2 since in the new optical design BS1 has no longer a 50% beam-splitter coating but a dichroic coating.

$F(\lambda)$ is the geometrical dilution factor related to the pupil illumination, considering the cone angle coming out from the mask pinholes (placeholder) and the cone angle associated to the LGS optical system f-numbers.

Table 21. Dilution factor related to the pupil illumination (LGS channels).

Channel	Pinhole $f_{\#}$	System $f_{\#}$	F
LGS-104	1.25	5.15	0.065
LGS-150	1.25	5.9	0.05

7.3 Throughput summary

The results of the throughput analysis for the different channels are reported in Table 22.

Table 22. Summary of the transmission values computed for the PUA channels.

	NGS-REF	NGS-LO/MIC	LGS
T_{LC}	0.69	0.74	0.74
T_{SS}	0.0063	0.045	0.132
T_{OS}	2.8 E-03	2.8 E-03	9.7 E-03
F	0.24	0.075	0.05
T	2.9 E-06	7.0 E-06	4.8 E-05

7.4 Lamps power and flux compliance

The typologies and main features of the physical sources (“Lamps”) selected for the CU are briefly reported below. In this section we verify for each source type the provided power with respect to the required power and, through their ratio, the compliance with respect to the requirements of maximum flux.

The selected NGS-REF “Lamp” has 10 mW of nominal power and spectral distribution as shown in Figure 45 left. The fraction of power emitted between 700 nm and 900 nm is ~16%, therefore we can consider 1.6 mW as “Lamp” power (P_{Lamp}).



The selected NGS-LO/MIC “Lamp” has 4.4 mW of max power and spectral distribution as shown in Figure 45 right. The fraction of power emitted between 1500 nm and 1800 (H band) nm is ~68%, therefore we can consider 3 mW as “Lamp” power (P_{Lamp}).

The selected LGS “Lamp” has 3.3 mW of min power and spectral distribution as shown in Figure 46. The fraction of power emitted between 585 nm and 594 nm is ~21% and we will use 5 lamps to feed the LightBox, therefore we consider 3.5 mW as “Lamp” power (P_{Lamp}).

The required power P_{req} has been computed considering the maximum flux required (N_{ph}) for each source type, as follows:

$$N_{ph} = \frac{\lambda_c}{h c} T P_{req} \Rightarrow P_{req} = \frac{h c N_{ph}}{\lambda_c T}$$

where λ_c is the central wavelength of each source and T is the total throughput.

For LGS, the provided power P_{prov} has been computed considering the number of calibration sources N fed by a single “Lamp”, as follows:

$$P_{prov} = \frac{P_{Lamp}}{N}$$

The power ratio P_{ratio} has been finally calculated as the ratio between P_{prov} and P_{req} and proves the fulfilment of the maximum flux requirement if sufficiently greater than 1. Data and results are summarized in Table 23.

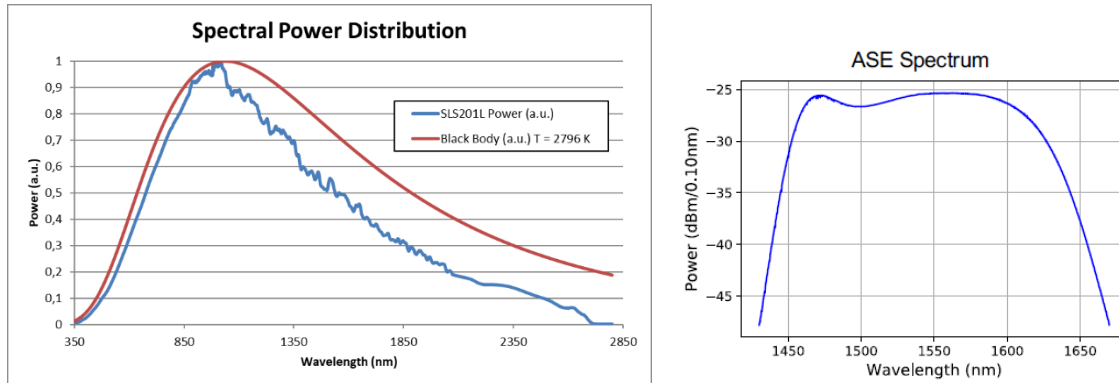


Figure 45. Spectral power distribution of (left) Thorlabs SL201L QTH lamp (fiber output) used for the NGS-REF sources (normalized distribution) and (right) EXALOS EXS210066-02 SLED (fiber output) used for the NGS-LO/MIC sources.

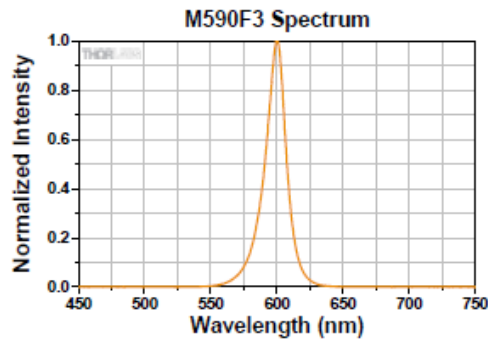


Figure 46. Spectral power distribution (normalized) of Thorlabs M590F3 laser (fiber output) used for the LGS sources.

Table 23. Verification of the CU sources flux. Compliance is verified for each source ($P_{ratio} > 1$). (*) No division is operated, as it is already taken into account by the splitters insertion losses (T_{ss}).

	NGS-REF	NGS-LO/MIC	LGS
N_{ph}^{max} [ph/s]	1.00E+08	5.00E+06	4.00E+10
T	2.9 E-06	7.0 E-06	4.8 E-05
Required Power P_{req} [mW/source]	1.3 E-03	5.2 E-06	1.4 E-02
P_{Lamp} [mW]	1.6	3	3.5
Sources q. ty (N)	32	16	12
Provided Power P_{prov} [mW/source]	1.6*	3*	0.29
P_{ratio}	189	4.34 E+04	1



8. Test Equipment

The PUA Test Equipment (TE) is an essential tool to ensure full accessibility to the CU output focal planes (both LGS and NGS) for enabling a comprehensive verification of the CU performance, taking into account the dimensions and volume constraints within the INAF integration rooms. It will be outsourced together with the PUA, therefore its final design and manufacturing (including the opto-mechanical components and a field scanning system) will be supplied by the Contractor. However, a concept for the TE has been preliminarily developed to allow understanding the needs underlying the definition of the requirements. The concept design (Figure 47) is aimed at reducing the TE overall size and minimizing the dimension of the auxiliary folding mirrors (AU-FM), hence reducing the complexity and the cost of this test tool. The required mechanics is basically a cage (similar to the MORFEO structure where PUA will be installed) with a movable optical bench on the top of it, provided with two pairs of motorized linear guides, to scan the full FoV the CU output focal planes.

According to the optical design of this concept, the LGS beams travel straight upwards along the Z direction after W, to reach the AU-FM1 that limits the overall height and redirect the light towards AU-FM2 (both mirrors are fixed). AU-FM2 bends the LGS light in the direction parallel to the bench (Y), where two more auxiliary mirrors, AU-FM3 and AU-FM4, are placed, and whose position depends on the test configuration used (LGS-104km, LGS-150km and NGS - see Figure 48). It is important to note that the size of all these mirrors is constrained by the LGS-104km optical path.

For the NGS beam, instead, a fifth auxiliary mirror, AU-FM5 is placed just above W, bending the light directly towards AU-FM3, therefore excluding AU-FM1 and AU-FM2.

Finally, a further specification for the TE is that it must be easily assembled and disassembled, shipped and used as needed during the various phases of the project.

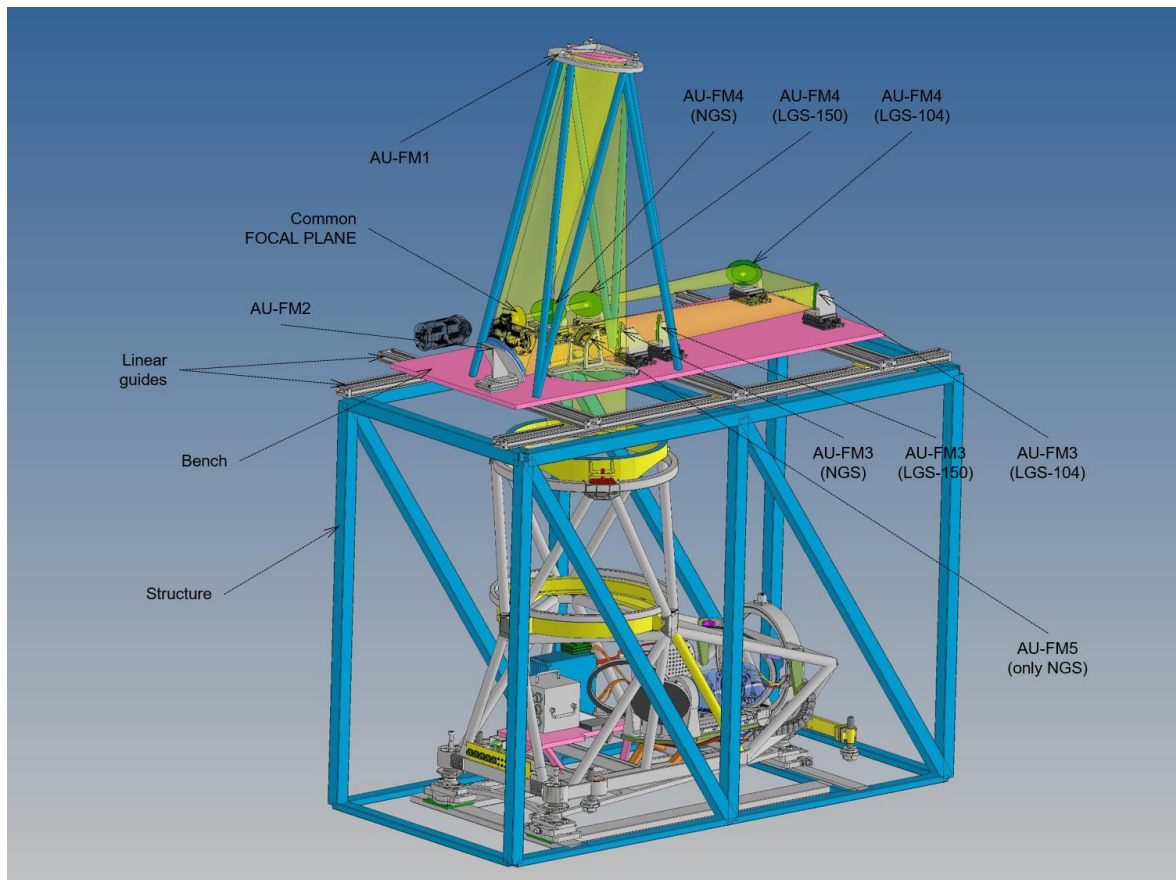


Figure 47. Test Equipment concept: overall layout.

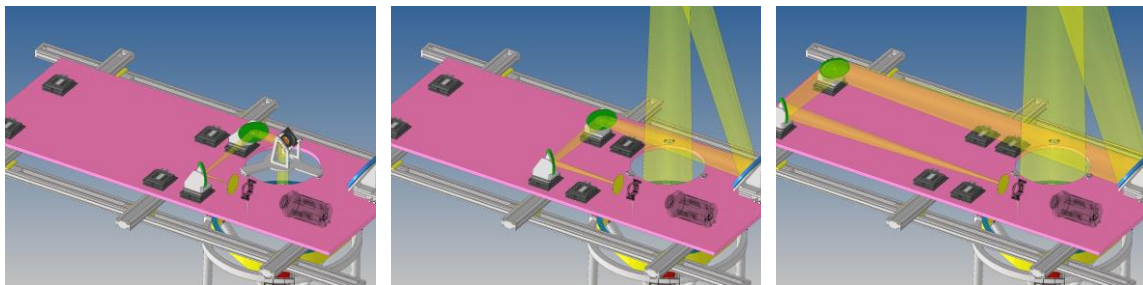


Figure 48. Test Equipment configurations according to the selected output beam: NGS (left), LGS-150km (center), LGS-104km (right).



9. Technical Risk Analysis

In this section the main technical risks related to the PUA-OFDR maturity level are presented. Severity and likelihood have been estimated and justified for each of them, as well as potential mitigation strategies. The severity of a risk refers to the potential impact or consequences that the risk event could have on the subsystem performances, if it were to occur. It is a critical aspect of risk assessment and helps in determining the priority and urgency of risk mitigation efforts. In this context, we foresee 4 possible levels of risk impacts, ranging from negligible to critical: Negligible (minimal or no impact), Significant (performance degradation), Major (Performance requirement(s) not met), Critical (Unacceptable performance). The risk level has been estimated assuming Table 24 as reference (medium risk is considered acceptable if associated with a proper mitigation strategy). For each risk, potential mitigation strategies have been evaluated.

Table 24. Risk assessment: reference table.

			SEVERITY SCALE			
			1	2	3	4
			Negligible	Significant	Major	Critical
LIKELIHOOD SCALE	E	Maximum (>80%)	Medium	High	High	High
	D	High (60%-80%)	Low	Medium	High	High
	C	Medium (30%-60%)	Low	Low	Medium	High
	B	Low (10%-30%)	Very Low	Low	Medium	High
	A	Minimum (<10%)	Very Low	Low	Medium	High

9.1 Ghost analysis

An extensive realistic ghost analysis was performed for the PDR (summarized in Section 5.5.1), considering preliminary opto-mechanics and basic baffling structures. Additional analyses have been performed for the OFDR (reported in Section 5.5.3). More detailed analyses will be performed by the Contractor for the FDR. Alignability tests against ghosts have been successfully carried out through the Calibration Unit paraxial prototype (PCUP) at INAF-OAAb.

Severity 2: A lower value of the source-to-ghost intensity ratio may lead to a worse performance.

Likelihood D: The dilute area factor is large enough to ensure a large margin with respect to the requirement.

Risk: MEDIUM

Mitigation: The full ray-tracing analysis will be carried out by the Contractor for FDR. This will assure schedule margin to optimize coatings and wedging to mitigate ghosts effect.



9.2 Stray-Light analysis

An extensive stray-light analysis was performed on the PUA for the PDR (summarized in Section 5.5.2). More detailed analyses will be performed by the Contractor for the FDR. Alignability tests and SNR estimations against stray-light have been successfully carried out through the PCUP at INAF-OAAb. It is sufficient to demonstrate that the assumed surface roughness has a negligible effect. Optical surface contamination is not well assessed at this working level as well as out-of-field cases.

Severity 2: A larger value of the scattered light by optical surfaces driven by roughness and contamination, and by mountings/structure and the ghost optical paths lead to an increment of the background signal.

Likelihood C: Given the amount of uncertainties at this working level (the detailed design is required for each opto-mechanical component and the contamination environment is not yet well understood), we will most probably need to address some unexpected background thresholds.

Risk: LOW

Mitigation:

- Proper baffling design, to be carried out by the Contractor;
- Protocol for optics periodic cleaning;
- A more sophisticated stray-light analysis (ray-tracing), to be performed by the Contractor for the FDR, considering the baffles designed for the purpose.

9.3 Throughput analysis

Throughput analysis is based on the current knowledge of the assumed coatings and material internal transmissivity, as well as on standard data and models for fibers, fiber splitters and lightbox. Real deposited coating, real glass substrate and laboratory tests on real transmission efficiency may lead to a worse efficiency performance.

Severity 3: Large departures from expected performances may lead to a significantly worse total throughput.

Likelihood B: The assumed values are based on company official datasheets or plots. However, some departure is expected.

Risk: MEDIUM

Mitigation: The throughput analyses show a good margin (at least a factor 10), which could be furtherly incremented using alternative solutions and/or physical sources. Additional analyses and lab test will be performed for FDR. Analysis on coatings and substrates will be carried out by the Contractor for the FDR and further increment of coating performance may be required after the design study, if needed.



9.4 CBS quality and procurement

The CBS is probably the most challenging optics of the PUA, for the homogeneity and surface optical quality required. Its procurement is another delicate aspect, since the blanks procurement, the prisms manufacturing, test and selection, the surfaces coating and the final gluing will likely be performed by different companies, with a large delivery time, as a consequence.

Severity 3: The CBS is a long-lead item and not all its technical specifications could be met, the CBS coating is critical as it defines the focal plane ghosts' brightness.

Likelihood C: According to the feedback received from potential providers, there is a concrete possibility that the homogeneity level of the CBS will be higher than that required and that the additional WFE introduced in the system will be significant.

Risk: MEDIUM

Mitigation:

- The CU OFDR is aimed at anticipating the call for tender conclusion and hence at ordering the CBS blanks at the beginning of the subsystem final design phase.
- More blanks will be ordered and several prisms will be manufactured and tested, with the best ones selected to have the best CBS and other two assembled to have a spare CBS.
- The WFE introduced by the CBS will be mostly defocus, WFE compensation strategy (Section 5.2.5) is potentially able to compensate any unwanted source of WFE coming from the CBS.
- Special coatings, such as Random Anti-Reflection coatings with a residual reflectivity smaller than 0.5%, would significantly dump focal plane ghosts.

9.5 Thermal effects

The NGS channel has no active elements to compensate for the defocus introduced by thermal displacements from the design temperature of 9°C.

Severity 2: if uncompensated, the thermal defocus would introduce a significant amount of WFE (defocus) for the NGS-REF and NGS-MIC channels.

Likelihood C: the foreseen thermal variations during daytime (when the CU is foreseen to operate) are limited to few degrees around the nominal value of 9°C.

Risk: LOW

Mitigation:

- Re-focusing will be performed at MORFEO-DMs level (Section 5.2.3), lookup tables have been retrieved from the PUA optical model with thermal pickups.
- Provision for axial motorization of the NGS mask, if needed.

9.6 Coatings

The baseline strategy foresees no re-coating for the PUA optical components.



Severity 2: The coatings aging could lead to a lower throughput, as well as to an increase of background (stray light) and, referring in particular to the CBS coating, to a presence of most powerful ghosts.

Likelihood C: considering the instrument life-time, a worsening of the throughput and delivered background seems unavoidable.

Risk: LOW

Mitigation:

- Pushing the general quality of the CBS coatings (the most critical ones – e.g., using Random Anti-Reflection coatings, with a residual reflectivity smaller than 0.5%), define a long life-time requirement on them.
- Establishing a cleaning procedure for the optics subjected to dust deposition (e.g. W).

9.7 Window aspect ratio

The thickness of the window W was reduced after PDR in order to save mass and lower the PUA CoG. The high aspect ratio (~21) translates into a high static deformation under gravity and potential difficulties during manufacturing.

Severity 2: The induced optical aberrations (mainly spherical aberrations and other related to types and amount of supports) have a significant impact on the delivered LGS channel WFE (large footprints on W).

Likelihood C: According to the preliminary feedbacks from manufacturers, the specifications are fine and can be met, however we still consider the high aspect ratio a potential risk and source of issues during the manufacturing process.

Risk: LOW

Mitigation: During the final design, if needed, we will agree with the Contractor a suitable increase of W thickness (an increase of 5 mm, for instance, would reduce by 25% the total sag and the spherical aberration associated to the gravitational deformation, with an increase of mass within 4 kg) and the consequent re-optimization of the optical design.

9.8 Alignment of W-SM

The tolerances defined for the alignment of the largest PUA optics (W and SM) are stringent (± 0.002 deg of tip/tilt for both). The sensitivity of the system to the tip/tilt residual alignment error of these large optics is quite high, especially for the LGS channels. The proposed W-SM alignment strategy relies on the use of the MAT and the degrees of freedom (tip/tilt) offered by the opto-mechanics of W, and on an interferometric feedback for the minimization of the residual WFE.

Severity 3: A larger value of the residual alignment error would introduce a significant amount of additional WFE, with a degradation of the PUA performance, as a consequence.

Likelihood C: The required positioning accuracy is achievable with the MAT in auto-collimation; nevertheless, besides some important aspects not yet detailed (such as the



resolution of the adjustments and the interferometric setup), there are some uncertainties related to the stability of the alignment achieved and, more in general, related to the alignment strategy itself, which might undergo some changes upon discussion with the Contractor.

Risk: MEDIUM

Mitigation:

- Close iteration with the Contractor to find the best solution to minimize the risk.
- Performing optical analyses more representative of the alignment steps and of the actual degrees of freedom and resolutions foreseen by the Contractor.



10. Verification Matrix

A complete verification and compliance matrix for the PUA specifications will be provided for FDR.



11. Conclusion

The Calibration Unit of MORFEO has entered the Final Design phase.

A deep revision process, started after the end of the PDR, made it possible to solve most of the criticalities of the preliminary design, thanks to an optical re-design that led to a new optical design (OFDR design), described in this document.

The mechanical re-design has been only preliminarily addressed: the final design will be outsourced. However, the design of some key mechanical sub-systems, such as the interface with the MORFEO Main Structure and the NGS and LGS mask assemblies, has been completed and the sub-systems are ready to be prototyped for laboratory tests.

The presence and impact of ghosts and stray light, the main drawback of the optical design, will be limited through proper coatings, baffles and vanes. The final design of coatings and baffling, as well as their implementation and complete ghost and stray light analysis, will be outsourced. For the time being, we consider valid the results of the analyses carried out for the PDR. The ghosts' presence has been verified and evaluated on the PUA paraxial prototype (PCUP), developed in INAF-OAAb lab.

The alignment strategy has been defined, as well as the main tests and verifications, both supported by the lab work carried out on the PCUP.

Tolerance analyses have been performed, to evaluate the impact of the surface irregularities in terms of WFE, this being one of the largest contributions to the WFE budget, and double-checking the tolerance values defined. Tolerance analyses have also been performed to check the overall effects on both WFE and exit pupil quality.

The WFE budget breakdown has been detailed and is dominated by the CBS overall contribution and by the contribution coming from the manufacturing tolerances (mainly surface irregularities) of the other optical elements. The tight/null margin with respect to the available NGS WFE budget suggests the need to implement a WFE compensation strategy, which has been clearly identified and proven to be effective.

The throughput analysis, performed considering the whole CU transmission chain, has shown the adequacy of the identified solutions and of the physical sources selected, although the margin for the LGS channels is very tight / null.

All the main technical risks have been assessed, and proper mitigation strategies identified.

***** End of document *****